HopSkipJumpAttack: A Query-Efficient Decision-Based Attack

Jianbo Chen[*], Michael I. Jordan[*], Martin J. Wainwright[*,†]

University of California, Berkeley[*], Voleon Group[†]

{jianbochen@, jordan@cs., wainwrig@}berkeley.edu

Abstract

The goal of a decision-based adversarial attack on a trained model is to generate adversarial examples based solely on observing output labels returned by the targeted model. We develop HopSkipJumpAttack[1], a family of algorithms based on a novel estimate of the gradient direction using binary information at the decision boundary. The proposed family includes both untargeted and targeted attacks optimized for ℓ_2 and ℓ_∞ similarity metrics respectively. Theoretical analysis is provided for the proposed algorithms and the gradient direction estimate. Experiments show HopSkipJumpAttack requires significantly fewer model queries than Boundary Attack. It also achieves competitive performance in attacking several widely-used defense mechanisms.

1 Introduction

Although deep neural networks have achieved state-of-the-art performance on a variety of tasks, they have been shown to be vulnerable to *adversarial examples*—that is, maliciously perturbed examples that are almost identical to original samples in human perception, but cause models to make incorrect decisions [1]. The vulnerability of neural networks to adversarial examples implies a security risk in applications with real-world consequences, such as self-driving cars, robotics, financial services, and criminal justice; in addition, it highlights fundamental differences between human learning and existing machine-based systems. The study of adversarial examples is thus necessary to identify the limitation of current machine learning algorithms, provide a metric for robustness, investigate the potential risk, and suggest ways to improve the robustness of models.

Recent years have witnessed a flurry of research on the design of new algorithms for generating adversarial examples [1–16]. Adversarial examples can be categorized according to at least three different criteria: the similarity metric, the attack goal, and the threat model. Commonly used similarity metrics are ℓ_p-distances between adversarial and original examples with $p \in \{0, 2, \infty\}$. The goal of attack is either untargeted or targeted. The goal of an untargeted attack is to perturb the input so as to cause any type of misclassification, whereas the goal of a targeted attack is to alter the decision of the model to a pre-specific target class. Changing the loss function allows for switching between two types of attacks [3, 5, 6].

Perhaps the most important criterion in practice is the *threat model*, of which there are two primary types: white-box and black-box. In the white-box setting, an attacker has complete access to the model, including its structure and weights. Under this setting, the generation of adversarial examples is often formulated as an optimization problem, which is solved either via treating misclassification loss as a regularization [1, 6] or via tackling the dual as a constrained optimization problem [2, 3, 7]. In the black-box setting, an attacker can only access outputs of the target model. Based on whether one has access to the full probability or the label of a given input, black-box attacks are further divided into score-based and decision-based. See Figure 1 for an illustration of accessible components of the target model for each of the three threat models. Chen et al. [8] and Ilyas et al. [9, 10] introduced score-based methods using zeroth-order gradient estimation to craft adversarial examples.

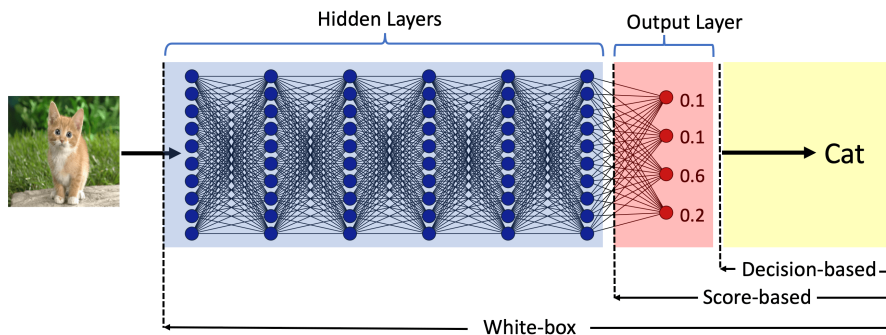[1]HopSkipJumpAttack was named Boundary Attack++ in a previous version of the preprint.

Figure 1. An illustration of accessible components of the target model for each of the three threat models. A white-box threat model assumes access to the whole model; a score-based threat model assumes access to the output layer; a decision-based threat model assumes access to the predicted label alone.

The most practical threat model is that in which an attacker has access to decisions alone. A widely studied type of the decision-based attack is transfer-based attack. Liu et al. [11] showed that adversarial examples generated on an ensemble of deep neural networks from a white-box attack can be transferred to an unseen neural network. Papernot et al. [12, 13] proposed to train a substitute model by querying the target model. However, transfer-based attack often requires a carefully-designed substitute model, or even access to part of the training data. Moreover, they can be defended against via training on a data set augmented by adversarial examples from multiple static pre-trained models [17]. In recent work, Brendel et al. [14] proposed Boundary Attack, which generates adversarial examples via rejection sampling. While relying neither on training data nor on the assumption of transferability, this attack method achieves comparable performance with state-of-the-art white-box attacks such as C&W attack [6]. One limitation of Boundary Attack, however, is that it was formulated only for ℓ_2-distance. Moreover, it requires a relatively large number of model queries, rendering it impractical for real-world applications.

It is more realistic to evaluate the vulnerability of a machine learning system under the decision-based attack with a limited budget of model queries. Online image classification platforms often set a limit on the allowed number of queries within a certain time period. For example, the cloud vision API from Google currently allow 1,800 requests per minute. Query inefficiency thus leads to clock-time inefficiency and prevents an attacker from carrying out large-scale attacks. A system may also be set to recognize the behavior of feeding a large number of similar queries within a small amount of time as a fraud, which will automatically filter out query-inefficient decision-based attacks. Last but not least, a smaller query budget directly implies less cost in evaluation and research. Query-efficient algorithms help save the cost of evaluating the robustness of public platforms, which incur a cost for each query made by the attacker. It also helps facilitate research in adversarial vulnerability, as such a decision-based attack which does not require access to model details may be used as a simple and efficient first step in evaluating new defense mechanisms, as we will see in Section 5.2 and 5.3.

In this paper, we study decision-based attacks under an optimization framework, and propose a novel family of algorithms for generating both targeted and untargeted adversarial examples that are optimized for minimum distance with respect to either the ℓ_2-distance or ℓ_∞ distance. The family of algorithms is iterative in nature, with each iteration involving three steps: estimation of the gradient direction, step-size search via geometric progression, and Boundary search via a binary search. Theoretical analysis has been carried out for the optimization framework and the gradient direction estimate, which not only provides insights for choosing hyperparamters, but also motivating essential steps in the proposed algorithms. We refer to the algorithm as HopSkipJumpAttack[2]. In summary, our contributions are the following:

- We propose a novel unbiased estimate of gradient direction at the decision boundary based solely on access to model decisions, and propose ways to control the error from deviation from the boundary.

---

[2]A hop, skip, and a jump originally referred to an exercise or game involving these movements dating from the early 1700s, but by the mid-1800s it was also being used figuratively for the short distance so covered.

- We design a family of algorithms, HopSkipJumpAttack, based on the proposed estimate and our analysis, which is hyperparameter-free, query-efficient and equipped with a convergence analysis.

- We demonstrate the superior efficiency of our algorithm over several state-of-the-art decision-based attacks through extensive experiments.

- Through the evaluation of several defense mechanisms such as defensive distillation, region-based classification, adversarial training and input binarization, we suggest our attack can be used as a simple and efficient first step for researchers to evaluate new defense mechanisms.

Roadmap. In Section 2, we describe previous work on decision-based adversarial attacks and their relationship to our algorithm. We also discuss the connection of our algorithm to zeroth-order optimization. In Section 3, we propose and analyze a novel iterative algorithm which requires access to the gradient information. Each step carries out a gradient update from the boundary, and then projects back to the boundary again. In Section 4, we introduce a novel asymptotically unbiased gradient-direction estimate at the boundary, and a binary-search procedure to approach the boundary. We also discuss how to control errors with deviation from the boundary. The analysis motivates a decision-based algorithm, HopSkipJumpAttack (Algorithm 2). Experimental results are provided in Section 5. We conclude in Section 6 with a discussion of future work.

2   Related work

2.1   Decision-based attacks

Most related to our work is the Boundary Attack method introduced by Brendel et al. [14]. Boundary Attack is an iterative algorithm based on rejective sampling, initialized at an image that lies in the target class. At each step, a perturbation is sampled from a proposal distribution, which reduces the distance of the perturbed image towards the original input. If the perturbed image still lies in the target class, the perturbation is kept. Otherwise, the perturbation is dropped. Boundary Attack achieves performance comparable to state-of-the-art white-box attacks on deep neural networks for image classification. The key obstacle to its practical application is, however, the demand for a large number of model queries. In practice, the required number of model queries for crafting an adversarial example directly determines the level of the threat imposed by a decision-based attack. One source of inefficiency in Boundary Attack is the rejection of perturbations which deviate from the target class. In our algorithm, the perturbations are used for estimation of a gradient direction.

Several other decision-based attacks have been proposed to improve efficiency. Brunner et al. [15] introduced Biased Boundary Attack, which biases the sampling procedure by combining low-frequency random noise with the gradient from a substitute model. Biased Boundary Attack is able to significantly reduce the number of model queries. However, it relies on the transferability between the substitute model and the target model, as with other transfer-based attacks. Our algorithm does not rely on the additional assumption of transferability. Instead, it achieves a significant improvement over Boundary Attack through the exploitation of discarded information into the gradient-direction estimation. Ilyas et al. [9] proposed Limited attack in the label-only setting, which directly performs projected gradient descent by estimating gradients based on novel proxy scores. Cheng et al. [16] introduced Opt attack, which transforms the original problem to a continuous version, and solves the new problem via randomized zeroth-order gradient update. Our algorithm approaches the original problem directly via a novel gradient-direction estimate, leading to improved query efficiency over both Limited Attack and Opt Attack. The majority of model queries in HopSkipJumpAttack come in mini-batches, which also leads to improved clock-time efficiency over Boundary Attack.

2.2   Zeroth-order optimization

Zeroth-order optimization refers to the problem of optimizing a function f based only on access to function values $f(x)$, as opposed to gradient values $\nabla f(x)$. Such problems have been extensively studied in the convex optimization and bandit literatures. Flaxman et al. [18] studied one-point randomized estimate of gradient for bandit convex optimization. Agarwal et al. [19] and Nesterov and Spokoiny [20] demonstrated that faster convergence can be achieved by using two function evaluations for estimating the gradient. Duchi et al. [21] established optimal rates of convex zeroth-order optimization via mirror descent with two-point gradient estimates. Zeroth-order algorithms have been applied to the generation of adversarial examples under the score-based threat model [8–10]. Subsequent work [22] proposed and analyzed an algorithm based on variance-reduced stochastic gradient estimates.

We formulate decision-based attack as an optimization problem. A core component of our proposed algorithm is a gradient-direction estimate, the design of which is motivated by zeroth-order optimization. However, the problem of decision-based attack is more challenging than zeroth-order optimization, essentially because we only have binary information from output labels of the target model, rather than function values.

3   An optimization framework

In this section, we describe an optimization framework for finding adversarial instances for an m-ary classification model of the following type. The first component is a *discriminant function* $F : \mathbb{R}^d \to \mathbb{R}^m$ that accepts an input $x \in [0,1]^d$ and produces an output $y \in \Delta_m := \{y \in [0,1]^m \mid \sum_{c=1}^m y_c = 1\}$. The output vector $y = (F_1(x), \ldots, F_m(x))$ can be viewed as a probability distribution over the label set $[m] = \{1, \ldots, m\}$. Based on the function F, the classifier $C : \mathbb{R}^d \to [m]$ assigns input x to the class with maximum probability—that is,

$$C(x) := \arg \max_{c \in [m]} F_c(x).$$

We study adversaries of both the untargeted and targeted varieties. Given some input $x^\star$, the goal of an *untargeted attack* is to change the original classifier decision $c^\star := C(x^\star)$ to any $c \in [m] \backslash \{c^\star\}$, whereas the goal of a *targeted attack* is to change the decision to some pre-specified $c^\dagger \in [m] \backslash \{c^\star\}$. Formally, if we define the function $S_{x^\star} : \mathbb{R}^d \to \mathbb{R}$ via

$$S_{x^\star}(x') := \begin{cases} \max_{c \neq c^\star} F_c(x') - F_{c^\star}(x') & \text{(Untargeted)} \\ F_{c^\dagger}(x') - \max_{c \neq c^\dagger} F_c(x') & \text{(Targeted)} \end{cases} \tag{1}$$

then a perturbed image x' is a successful attack if and only if $S_{x^\star}(x') > 0$. The boundary between successful and unsuccessful perturbed images is

$$\text{bd}(S_{x^\star}) := \left\{ z \in [0,1]^d \mid S_{x^\star}(z) = 0 \right\}.$$

As an indicator of successful perturbation, we introduce the Boolean-valued function $\phi_{x^\star} : [0,1]^d \to \{-1, 1\}$ via

$$\phi_{x^\star}(x') := \text{sign}\left(S_{x^\star}(x')\right) = \begin{cases} 1 & \text{if } S_{x^\star}(x') > 0, \\ -1 & \text{otherwise.} \end{cases}$$

This function is accessible in the decision-based setting, as it can be computed by querying the classifier C alone. The goal of an adversarial attack is to generate a perturbed sample x' such that $\phi_{x^\star}(x') = 1$, while keeping x' close to the original sample $x^\star$. This can be formulated as the optimization problem

$$\min_{x'} d(x', x^\star) \quad \text{such that} \quad \phi_{x^\star}(x') = 1, \tag{2}$$

where d is a distance function that quantifies similarity. Standard choices of d studied in past work [5, 2, 6] include the usual ℓ_p-norms, for $p \in \{0, 2, \infty\}$.

3.1 An iterative algorithm for ℓ_2 distance

Consider the case of the optimization problem (2) with the ℓ_2-norm $d(x, x^\star) = \|x - x^\star\|_2$. We first specify an iterative algorithm that is given access to the gradient $\nabla S_{x^\star}$. Given an initial vector x_0 such that $S_{x^\star}(x_0) > 0$ and a stepsize sequence $\{\xi_t\}_{t \geq 0}$, it performs the update

$$x_{t+1} = \alpha_t x^\star + (1 - \alpha_t) \left\{ x_t + \xi_t \frac{\nabla S_{x^\star}(x_t)}{\|\nabla S_{x^\star}(x_t)\|_2} \right\}, \tag{3}$$

where ξ_t is a positive step size. Here the line search parameter $\alpha_t \in [0, 1]$ is chosen such that $S_{x^\star}(x_{t+1}) = 0$—that is, so that the next iterate x_{t+1} lies on the boundary. The motivation for this choice is that our gradient-direction estimate in Section 4 is only valid near the boundary.

We now analyze this algorithm with the assumption that we have access to the gradient of $S_{x^\star}$ in the setting of binary classification. Assume that the function $S_{x^\star}$ is twice differentiable with a locally Lipschitz gradient, meaning that there exists $L > 0$ such that for all $x, y \in \{z : \|z - x^\star\|_2 \leq \|x_0 - x^\star\|_2\}$, we have

$$\|\nabla S_{x^\star}(x) - \nabla S_{x^\star}(y)\|_2 \leq L \|x - y\|_2, \tag{4}$$

where x_0 is the initialization point. In addition, we assume the gradient is bounded away from zero on the boundary: there exists a positive $c > 0$ such that $\|\nabla S_{x^\star}(z)\| > c$ for any $z \in \mathrm{bd}(S_{x^\star})$.

We analyze the behavior of the updates (3) in terms of the angular measure

$$r(x_t, x^\star) := \cos \angle (x_t - x^\star, \nabla S_{x^\star}(x_t))$$
$$= \frac{\langle x_t - x^\star, \, \nabla S_{x^\star}(x_t) \rangle}{\|x_t - x^\star\|_2 \|\nabla S_{x^\star}(x_t)\|_2},$$

corresponding to the cosine of the angle between $x_t - x^\star$ and the gradient $\nabla S_{x^\star}(x_t)$. Note that the condition $r(x, x^\star) = 1$ holds if and only if x is a stationary point of the optimization (2). The following theorem guarantees that, with a suitable step size, the updates converge to such a stationary point:

Theorem 1. *Under the previously stated conditions on $S_{x^\star}$, suppose that we compute the updates* (3) *with the step size* $\xi_t = \|x_t - x^\star\|_2 t^{-q}$ *for some* $q \in \left(\frac{1}{4}, \frac{1}{2} \right)$. *Then there is a universal constant c such that*

$$0 \leq 1 - r(x_t, x^\star) \leq c \, \frac{1}{t^{\frac{1}{2} - q}} \quad \text{for all iterations } t = 1, 2, \ldots . \tag{5}$$

In particular, the algorithm converges to a stationary point of problem (2).

Theorem 1 suggests a scheme for choosing the step size in the algorithm that we present in the next section. An experimental evaluation of the proposed scheme is carried out in Section 5.4. The proof of the theorem is constructed by establishing the relationship between the objective value $d(x_t, x^\star)$ and $r(x_t, x^\star)$, with a second-order Taylor approximation to the boundary. See Appendix A.1 for details.

3.2 Extension to ℓ_∞-distance

We now describe how to extend these updates so as to minimize the ℓ_∞-distance. Consider the ℓ_2-projection of a point x onto the sphere of radius α_t centered at $x^\star$:

$$\Pi_{x^\star, \alpha_t}^2(x) := \underset{\|y - x^\star\|_2 \leq \alpha_t}{\arg \min} \|y - x\|_2 = \alpha_t x^\star + (1 - \alpha_t)x. \tag{6}$$

In terms of this operator, our ℓ_2-based update (3) can be rewritten in the equivalent form

$$x_{t+1} = \Pi^2_{x^\star,\alpha_t}\left(x_t + \xi_t \frac{\nabla S_{x^\star}(x_t)}{\|\nabla S_{x^\star}(x_t)\|_2}\right). \tag{7}$$

This perspective allows us to extend the algorithm to other ℓ_p-norms for $p \neq 2$. For instance, in the case $p = \infty$, we can define the ℓ_∞-projection operator $\Pi^\infty_{x^\star,\alpha}$. It performs a per-pixel clip within a neighborhood of $x^\star$, such that the ith entry of $\Pi^\infty_{x^\star,\alpha}(x)$ is

$$\Pi^\infty_{x^\star,\alpha}(x)_i := \max\left\{\min\{x_i^\star, x_i^\star + c\}, x_i - c\right\},$$

where $c := \alpha\|x - x^\star\|_\infty$. We propose the ℓ_∞-version of our algorithm by carrying out the following update iteratively:

$$x_{t+1} = \Pi^\infty_{x^\star,\alpha_t}\left(x_t + \xi_t \text{sign}(\nabla S_{x^\star}(x_t))\right), \tag{8}$$

where α_t is chosen such that $S_{x^\star}(x_{t+1}) = 0$, and "sign" returns the element-wise sign of a vector. We use the sign of the gradient for faster convergence in practice, similar to previous work [2, 3, 7]. We also provide a detailed discussion on the connection of our optimization framework with existing white-box algorithms in Appendix B.

4   A decision-based algorithm based on a novel gradient estimate

We now extend our procedures to the decision-based setting, in which we have access *only* to the Boolean-valued function $\phi_{x^\star}(x) = \text{sign}(S_{x^\star}(x))$—that is, the method cannot observe the underlying discriminant function F or its gradient. In this section, we introduce a gradient-direction estimate based on $\phi_{x^\star}$ when $x_t \in \text{bd}(S_{x^\star})$ (so that $S_{x^\star}(x_t) = 0$ by definition). We proceed to discuss how to approach the boundary. Then we discuss how to control the error of our estimate with a deviation from the boundary. We will summarize the analysis with a decision-based algorithm.

4.1   At the boundary

Given an iterate $x_t \in \text{bd}(S_{x^\star})$ we propose to approximate the direction of the gradient $\nabla S_{x^\star}(x_t)$ via the Monte Carlo estimate

$$\widetilde{\nabla S}(x_t, \delta) := \frac{1}{B}\sum_{b=1}^{B}\phi_{x^\star}(x_t + \delta u_b)u_b, \tag{9}$$

where $\{u_b\}_{b=1}^{B}$ are i.i.d. draws from the uniform distribution over the d-dimensional sphere, and δ is small positive parameter. (The dependence of this estimator on the fixed centering point $x^\star$ is omitted for notational simplicity.)

The perturbation parameter δ is necessary, but introduces a form of bias in the estimate. Our first result controls this bias, and shows that $\widetilde{\nabla S}(x_t, \delta)$ is asymptotically unbiased as $\delta \to 0^+$.

Theorem 2. *For a boundary point x_t, suppose that $S_{x^\star}$ has L-Lipschitz gradients in a neighborhood of x_t. Then the cosine of the angle between $\widetilde{\nabla S}(x_t, \delta)$ and $\nabla S_{x^\star}(x_t)$ is bounded as*

$$\cos\angle\left(\mathbb{E}[\widetilde{\nabla S}(x_t, \delta)], \nabla S_{x^\star}(x_t)\right) \geq 1 - \frac{9L^2\delta^2 d^2}{8\|\nabla S(x_t)\|_2^2}. \tag{10}$$

In particular, we have

$$\lim_{\delta \to 0}\cos\angle\left(\mathbb{E}[\widetilde{\nabla S}(x_t, \delta)], \nabla S_{x^\star}(x_t)\right) = 1, \tag{11}$$

showing that the estimate is asymptotically unbiased as an estimate of direction.

We remark that Theorem 2 only establishes the asymptotic behavior of the proposed estiamte at the boundary. This also motivates the boundary search step in our algorithm to be discussed in Seciton 4.2. The proof of Theorem 2 starts from dividing the unit sphere into three components: the upper cap along the direction of gradient, the lower cap opposite to the direction of gradient, and the annulus in between. The error from the annulus can be bounded when δ is small. See Appendix A.2 for the proof of this theorem. As will be seen in the sequel, the size of perturbation δ should be chosen proportionally to d^{-1}; see Section 4.3 for details.

4.2   Approaching the boundary

The proposed estimate (9) is only valid at the boundary. We now describe how we approach the boundary via a binary search. Let $\tilde{x}_t$ denote the updated sample before the operator Π^p_{x,α_t} is applied:

$$\tilde{x}_t := x_t + \xi_t v_t(x_t, \delta_t), \text{ such that} \tag{12}$$

$$v_t(x_t, \delta_t) = \begin{cases} \widehat{\nabla S}(x_t, \delta_t)/\|\widehat{\nabla S}(x_t, \delta_t)\|_2, \text{ if } p = 2, \\ \text{sign}(\widehat{\nabla S}(x_t, \delta_t)), \text{ if } p = \infty, \end{cases}$$

where $\widehat{\nabla S}$ will be introduced later in equation (16), as a variance-reduced version of $\widehat{\nabla S}$, and δ_t is the size of perturbation at the t-th step.

We hope $\tilde{x}_t$ is at the opposite side of the boundary to x so that the binary search can be carried out. Therefore, we initialize at $\tilde{x}_0$ at the target side with $\phi_{x^\star}(\tilde{x}_0) = 1$, and set $x_0 := \Pi^p_{x,\alpha_0}(\tilde{x}_0)$, where α_0 is chosen via a binary search between 0 and 1 to approach the boundary, stopped at x_0 lying on the target side with $\phi_{x^\star}(x_0) = 1$. At the t-th iteration, we start at x_t lying at the target side $\phi_{x^\star}(x_t) = 1$. The step size is initialized as

$$\xi_t := \|x_t - x^\star\|_p/\sqrt{t}, \tag{13}$$

as suggested by Theorem 1 in the ℓ_2 case, and is decreased by half until $\phi_{x^\star}(\tilde{x}_t) = 1$, which we call *geometric progression* of ξ_t. Having found an appropriate $\tilde{x}_t$, we choose the projection radius α_t via a binary search between 0 and 1 to approach the boundary, which stops at x_{t+1} with $\phi_{x^\star}(x_{t+1}) = 1$. See Algorithm 1 for the complete binary search, where the binary search threshold θ is set to be some small constant.

Algorithm 1 Bin-Search

Require: Samples x', x, with a binary function ϕ, such that $\phi(x') = 1, \phi(x) = 0$, threshold θ, constraint ℓ_p.
Ensure: A sample x'' near the boundary.
  Set $\alpha_l = 0$ and $\alpha_u = 1$.
  while $|\alpha_l - \alpha_u| > \theta$ **do**
    Set $\alpha_m \leftarrow \frac{\alpha_l + \alpha_u}{2}$.
    if $\phi(\Pi_{x,\alpha_m}(x')) = 1$ **then**
      Set $\alpha_u \leftarrow \alpha_m$.
    else
      Set $\alpha_l \leftarrow \alpha_m$.
    end if
  end while
  Output $x'' = \Pi_{x,\alpha_u}(x')$.

4.3   Controlling errors of deviations from the boundary

Binary search never places x_{t+1} exactly onto the boundary. We analyze the error of the gradient-direction estimate, and propose two approaches for reducing the error.

Appropriate choice of the size of random perturbation   First, the size of random perturbation δ_t for estimating the gradient direction is chosen as a function of image size d and the binary search threshold θ. This is different from numerical differentiation, where the optimal choice of δ_t is at the scale of round-off errors (e.g., [23]). Below we characterize the error incurred by a large δ_t as a function of distance between $\tilde{x}_t$ and the boundary, and derive the appropriate choice of ξ_t and δ_t. In fact, with a Taylor approximation of $S_{x^\star}$ at x_t, we have

$$S_{x^\star}(x_t + \delta_t u) = S_{x^\star}(x_t) + \delta_t \langle \nabla S_{x^\star}(x_t),\, u \rangle + \mathcal{O}(\delta_t^2).$$

At the boundary $S_{x^\star}(x_t) = 0$, the error of gradient approximation scales at $\mathcal{O}(\delta_t^2)$, which is minimized by reducing δ_t to the scale of rooted round-off error. However, the outcome x_t of a finite-step binary search lies close to, but not exactly on the boundary.

When δ_t is small enough such that second-order terms can be omitted, the first-order Taylor approximation implies that $\phi_{x^\star}(x_t + \delta_t u) = -1$ if and only if $x_t + \delta_t u$ lies on the spherical cap $\mathcal{C}$, with

$$\mathcal{C} := \left\{ u \mid \left\langle \frac{\nabla S_{x^\star}(x_t)}{\|\nabla S_{x^\star}(x_t)\|_2},\, u \right\rangle < -\delta_t^{-1} \frac{S_{x^\star}(x_t)}{\|\nabla S_{x^\star}(x_t)\|_2} \right\}.$$

On the other hand, the probability mass of u concentrates on the equator in a high-dimensional sphere, which is characterized by the following inequality [24]:

$$\mathbb{P}(u \in \mathcal{C}) \leq \frac{2}{c} \exp\{-\frac{c^2}{2}\}, \text{ where } c = \frac{\sqrt{d-2} S_{x^\star}(x_t)}{\delta_t \|\nabla S_{x^\star}(x_t)\|_2}. \tag{14}$$

A Taylor expansion of x_t at $x_t' := \Pi_\partial^2(x_t)$ yields

$$S_{x^\star}(x_t) = \nabla S_{x^\star}(x_t')^T (x_t - x_t') + \mathcal{O}(\|x_t - x_t'\|_2^2)$$
$$= \nabla S_{x^\star}(x_t)^T (x_t - x_t') + \mathcal{O}(\|x_t - x_t'\|_2^2).$$

By the Cauchy-Schwarz inequality and the definition of ℓ_2-projection, we have

$$|\nabla S_{x^\star}(x_t)^T (x_t - x_t')|$$
$$\leq \|\nabla S_{x^\star}(x_t)\|_2 \|x_t - \Pi_\partial^2(x_t)\|_2$$
$$\leq \begin{cases} \|\nabla S_{x^\star}(x_t)\|_2 \theta \|\tilde{x}_{t-1} - x^\star\|_p, & \text{if } p = 2, \\ \|\nabla S_{x^\star}(x_t)\|_2 \theta \|\tilde{x}_{t-1} - x^\star\|_p \sqrt{d}, & \text{if } p = \infty. \end{cases}$$

This yields

$$c = \mathcal{O}\left(\frac{d^q \theta \|\tilde{x}_{t-1} - x^\star\|_p}{\delta_t}\right),$$

where $q = 1 - (1/p)$ is the dual exponent. In order to avoid a loss of accuracy from concentration of measure, we let $\delta_t = d^q \theta \|\tilde{x}_{t-1} - x^\star\|_2$. To make the approximation error independent of dimension d, we set θ at the scale of d^{-q-1}, so that δ_t is proportional to d^{-1}, as suggested by Theorem 2. This leads to a logarithmic dependence on dimension for the number of model queries. In practice, we set

$$\theta = d^{-q-1};\ \delta_t = d^{-1}\|\tilde{x}_{t-1} - x^\star\|_p. \tag{15}$$

A baseline for variance reduction in gradient-direction estimation   Another source of error comes from the variance of the estimate, where we characterize variance of a random vector $v \in \mathbb{R}^d$ by the trace of its covariance operator: $\mathrm{Var}(v) :=$

Algorithm 2 HopSkipJumpAttack

Require: Classifier C, a sample x, constraint ℓ_p, initial batch size B_0, iterations T.
Ensure: Perturbed image x_t.
  Set θ (Equation (15)).
  Initialize at $\tilde{x}_0$ with $\phi_{x^\star}(\tilde{x}_0) = 1$.
  Compute $d_0 = \|\tilde{x}_0 - x^\star\|_p$.
  for t in $1, 2, \ldots, T-1$ **do**
    (**Boundary search**)
    $x_t = \text{BIN-SEARCH}(\tilde{x}_{t-1}, x, \theta, \phi_{x^\star}, p)$
    (**Gradient-direction estimation**)
    Sample $B_t = B_0\sqrt{t}$ unit vectors $u_1, \ldots, u_{B_t}$.
    Set δ_t (Equation (15)).
    Compute $v_t(x_t, \delta_t)$ (Equation (12)).
    (**Step size search**)
    Initialize step size $\xi_t = \|x_t - x^\star\|_p/\sqrt{t}$.
    while $\phi_{x^\star}(x_t + \varepsilon_t v_t) = 0$ **do**
      $\xi_t \leftarrow \xi_t/2$.
    end while
    Set $\tilde{x}_t = x_t + \xi_t v_t$.
    Compute $d_t = \|\tilde{x}_t - x^\star\|_p$.
  end for
  Output $x_t = \text{BIN-SEARCH}(\tilde{x}_{t-1}, x, \theta, \phi_{x^\star}, p)$.

$\sum_{i=1}^{d} \text{Var}(v_i)$. When x_t deviates from the boundary and δ_t is not exactly zero, there is an uneven distribution of perturbed samples at the two sides of the boundary:

$$|\mathbb{E}[\phi_{x^\star}(x_t + \delta_t u)]| > 0,$$

as we can see from Equation (14). To attempt to control the variance, we introduce a baseline $\overline{\phi_{x^\star}}$ into the estimate:

$$\overline{\phi_{x^\star}} := \frac{1}{B}\sum_{b=1}^{B} \phi_{x^\star}(x_t + \delta u_b),$$

which yields the following estimate:

$$\widehat{\nabla S}(x_t, \delta) := \frac{1}{B-1}\sum_{b=1}^{B}(\phi_{x^\star}(x_t + \delta u_b) - \overline{\phi_{x^\star}})u_b. \tag{16}$$

It can be easily observed that this estimate is equal to the previous estimate in expectation, and thus still asymptotically unbiased at the boundary: When $x_t \in \text{bd}(S_{x^\star})$, we have

$$\cos\angle\left(\mathbb{E}[\widehat{\nabla S}(x_t, \delta)], \nabla S_{x^\star}(x_t)\right) \geq 1 - \frac{9L^2\delta^2 d^2}{8\|\nabla S(x_t)\|_2^2},$$

$$\lim_{\delta \to 0} \cos\angle\left(\mathbb{E}[\widehat{\nabla S}(x_t, \delta)], \nabla S_{x^\star}(x_t)\right) = 1.$$

Moreover, the introduction of the baseline reduces the variance when $\mathbb{E}[\phi_{x^\star}(x_t + \delta u)]$ deviates from zero. In particular, the following theorem shows that whenever $|\mathbb{E}[\phi_{x^\star}(x_t + \delta u)]| = \Omega(B^{-\frac{1}{2}})$, the introduction of a baseline reduces the variance.

Theorem 3. *Defining $\sigma^2 := Var(\phi_{x^\star}(x_t + \delta u)u)$ as the variance of one-point estimate, we have*

$$Var(\widehat{\nabla S}(x_t, \delta)) < Var(\widetilde{\nabla S}(x_t, \delta))(1 - \psi),$$

where

$$\psi = \frac{2}{\sigma^2(B-1)}\left(2B\mathbb{E}[\phi_{x^\star}(x_t + \delta u)]^2 - 1\right) - \frac{2B-1}{(B-1)^2}.$$
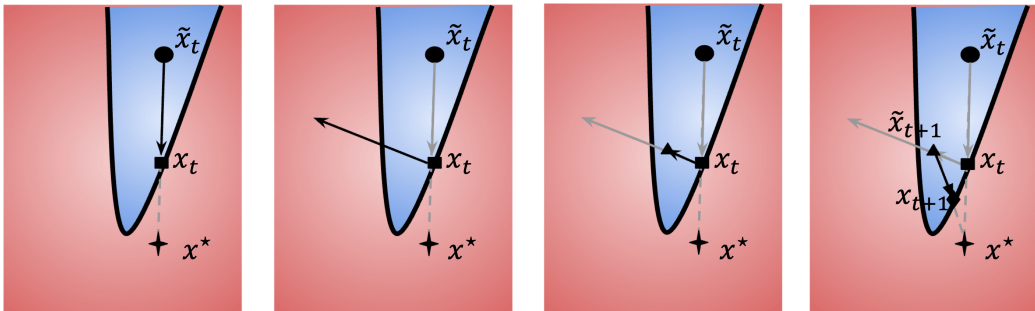
Figure 2. Intuitive explanation of HopSkipJumpAttack. (a) Perform a binary search to find the boundary, and then update $\tilde{x}_t \rightarrow x_t$. (b) Estimate the gradient at the boundary point x_t. (c) Geometric progression and then update $x_t \rightarrow \tilde{x}_{t+1}$. (d) Perform a binary search, and then update $\tilde{x}_{t+1} \rightarrow x_{t+1}$.

See Appendix A.3 for the proof. We also present an experimental evaluation of our gradient-direction estimate when the sample deviates from the boundary in Section 5.4, where we show our proposed choice of δ_t and the introduction of baseline yield a performance gain in estimating gradient.

4.4   HopSkipJumpAttack

We now combine the above analysis into an iterative algorithm, HopSkipJumpAttack. It is initialized with a sample in the target class for untargeted attack, and with a sample blended with uniform noise that is misclassified for targeted attack. Each iteration of the algorithm has three components. First, the iterate from the last iteration is pushed towards the boundary via a binary search (Algorithm 1). Second, the gradient direction is estimated via Equation (16). Third, the updating step size along the gradient direction is initialized as Equation (13) based on Theorem 1, and is decreased via geometric progression until perturbation becomes successful. The next iteration starts with projecting the perturbed sample back to the boundary again. The complete procedure is summarized in Algorithm 2. Figure 2 provides an intuitive visualization of the three steps in ℓ_2. For all experiments, we initialize the batch size at 100 and increase it with $\sqrt{t}$ linearly, so that the variance of the estimate reduces with t. When the input domain is bounded in practice, a clip is performed at each step by default.

5   Experiments

In this section, we carry out experimental analysis of HopSkipJumpAttack. We compare the efficiency of HopSkipJumpAttack with several previously proposed decision-based attacks on image classification tasks. In addition, we evaluate the robustness of three defense mechanisms under our attack method. We also evaluate the performance of HopSkipJumpAttack on models without gradients. Finally, we carry out sensitivity analysis to validate the choice of hyperparameters suggested by previous analysis. All experiments were carried out on a Tesla K80 GPU, with code for the experiments available on GitHub[3]. Our algorithm is also available on CleverHans [25] and Foolbox [26], which are two popular Python packages to craft adversarial examples for machine learning models.

---

[3]https://github.com/Jianbo-Lab/HSJA

Table 1. Median distance at various model queries. The smaller median distance at a given model query is bold-faced. BA and HSJA stand for Boundary Attack and HopSkipJumpAttack respectively.

Distance	Data	Model	Objective	Model Queries								
				1K			5K			20K		
				BA	Opt	HSJA	BA	Opt	HSJA	BA	Opt	HSJA
ℓ_2	MNIST	CNN	Untargeted	6.14	6.79	**2.46**	5.45	3.76	**1.67**	1.50	2.07	**1.48**
			Targeted	5.41	4.84	**3.26**	5.38	3.90	**2.24**	1.98	2.49	**1.96**
	CIFAR10	ResNet	Untargeted	2.78	2.07	**0.56**	2.34	0.77	**0.21**	0.27	0.29	**0.13**
			Targeted	7.83	8.21	**2.53**	5.91	4.76	**0.41**	0.59	1.06	**0.21**
		DenseNet	Untargeted	2.57	1.78	**0.48**	2.12	0.67	**0.18**	0.21	0.28	**0.12**
			Targeted	7.70	7.65	**1.75**	5.33	3.47	**0.34**	0.35	0.78	**0.19**
	CIFAR100	ResNet	Untargeted	1.34	1.20	**0.20**	1.12	0.41	**0.08**	0.10	0.14	**0.06**
			Targeted	9.30	12.43	**6.12**	7.40	8.34	**0.92**	1.61	4.06	**0.29**
		DenseNet	Untargeted	1.47	1.22	**0.25**	1.23	0.34	**0.11**	0.12	0.13	**0.08**
			Targeted	8.83	11.72	**5.10**	6.76	8.22	**0.75**	0.91	2.89	**0.26**
	ImageNet	ResNet	Untargeted	36.86	33.60	**9.75**	31.95	13.91	**2.30**	2.71	5.26	**0.84**
			Targeted	87.49	84.38	**71.99**	82.91	71.83	**38.79**	40.92	53.78	**10.95**
ℓ_∞	MNIST	CNN	Untargeted	0.788	0.641	**0.235**	0.700	0.587	**0.167**	0.243	0.545	**0.136**
			Targeted	0.567	0.630	**0.298**	0.564	0.514	**0.211**	0.347	0.325	**0.175**
	CIFAR10	ResNet	Untargeted	0.127	0.128	**0.023**	0.105	0.096	**0.008**	0.019	0.073	**0.005**
			Targeted	0.379	0.613	**0.134**	0.289	0.353	**0.028**	0.038	0.339	**0.010**
		DenseNet	Untargeted	0.114	0.119	**0.017**	0.095	0.078	**0.007**	0.017	0.063	**0.004**
			Targeted	0.365	0.629	**0.130**	0.249	0.359	**0.022**	0.025	0.338	**0.008**
	CIFAR100	ResNet	Untargeted	0.061	0.077	**0.009**	0.051	0.055	**0.004**	0.008	0.040	**0.002**
			Targeted	0.409	0.773	**0.242**	0.371	0.472	**0.124**	0.079	0.415	**0.019**
		DenseNet	Untargeted	0.065	0.076	**0.010**	0.055	0.038	**0.005**	0.010	0.030	**0.003**
			Targeted	0.388	0.750	**0.248**	0.314	0.521	**0.096**	0.051	0.474	**0.017**
	ImageNet	ResNet	Untargeted	0.262	0.287	**0.057**	0.234	0.271	**0.017**	0.030	0.248	**0.007**
			Targeted	0.615	0.872	**0.329**	0.596	0.615	**0.219**	0.326	0.486	**0.091**

5.1   Efficiency evaluation

Baselines   We compare HopSkipJumpAttack with three state-of-the-art decision-based attacks: Boundary Attack [14], Limited Attack [9] and Opt Attack [16]. We use the implementation of the three algorithms with the suggested hyper-parameters from the publicly available source code online. Limited Attack is only included under the targeted ℓ_∞ setting.

Data and models   For a comprehensive evaluation of HopSkipJumpAttack, we use a wide range of data and models, with varied image dimensions, data set sizes, complexity levels of task and model structures. The experiments are carried out over four image data sets: MNIST, CIFAR-10 [27], CIFAR-100 [27], and ImageNet [28] with the standard train/test split [29]. The four data sets have varied image dimensions and class numbers. MNIST contains 70K 28×28 gray-scale images of handwritten digits in the range 0-9. CIFAR-10 and CIFAR-100 are both composed of $32 \times 32 \times 3$ images. CIFAR-10 has 10 classes, with 6K images per class, while CIFAR-100 has 100 classes, with 600 images per class. ImageNet has $1,000$ classes. Images in ImageNet are rescaled to $224 \times 224 \times 3$. For MNIST, CIFAR-10 and CIFAR-100, $1,000$ correctly classified test images are used, which are randomly drawn from the test data set, and evenly distributed across classes. For ImageNet, we use 100 correctly classified test images, evenly distributed among 10 randomly selected classes. The selection scheme follows Metzen et al. [30] for reproducibility.

We also use models of varied structure, from simple to complex. For MNIST, we use a simple convolutional network composed of two convolutional layers followed by a hidden dense layer with 1024 units. Two convolutional layers have $32, 64$ filters respectively, each of which is followed by a max-pooling layer. For both CIFAR-10 and CIFAR-100, we train a 20-
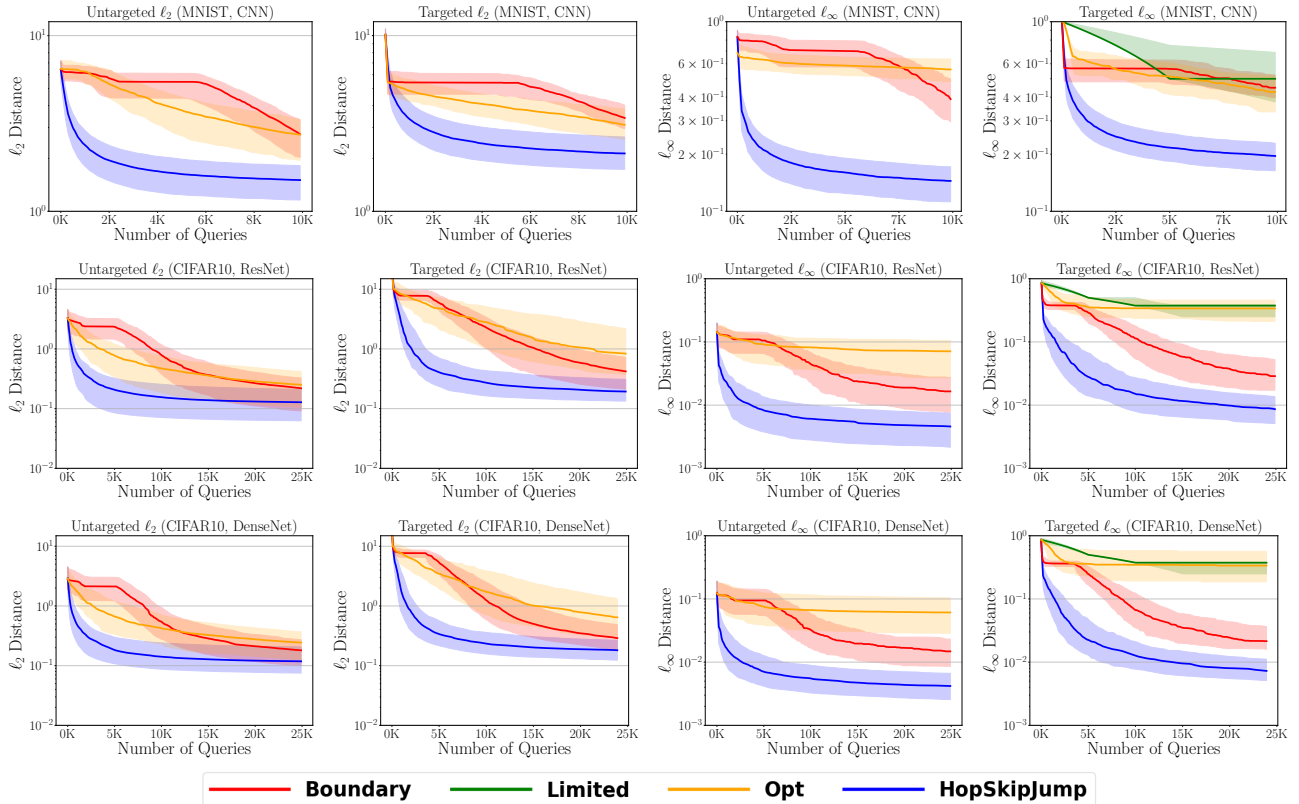
Figure 3. Median distance versus number of model queries on MNIST with CNN, and CIFAR-10 with ResNet and DenseNet from top to bottom rows. 1st column: untargeted ℓ_2. 2nd col.: targeted ℓ_2. 3rd col.: untargeted ℓ_∞. 4th col.: targeted ℓ_∞.

layer ResNet [31] and 121-layer DenseNet [32] respectively, with the canonical network structure [29]. For ImageNet, we use a pre-trained 50-layer ResNet [31]. All models achieve close to state-of-the-art accuracy on the respective data set. All pixels are scaled to be in the range $[0, 1]$. For all experiments, we clip the perturbed image into the input domain $[0, 1]$ for all algorithms by default.

Initialization   For untargeted attack, we initialize all attacks by blending an original image with uniform random noise, and increasing the weight of uniform noise gradually until it is misclassified, a procedure which is available on a widely-used python package, Foolbox [26], as the default initialization of Boundary Attack. For targeted attack, the target class is sampled uniformly among the incorrect labels. An image belonging to the target class is randomly sampled from the test set as the initialization. The same target class and a common initialization image are used for all attacks.

Metrics   The first metric is the median ℓ_p distance between perturbed and original samples over a subset of test images, which was commonly used in previous work, such as Carlini and Wagner [6]. A version normalized by image dimension was employed by Brendel et al. [14] for evaluating Boundary Attack. The ℓ_2 distance can be interpreted in the following way: Given a byte image of size $h \times w \times 3$, perturbation of size d in ℓ_2 distance on the rescaled input image amounts to perturbation on the original image of $\lceil d/\sqrt{h \times w \times 3} * 255 \rceil$ bits per pixel on average, in the range $[0, 255]$. The perturbation of size d in ℓ_∞ distance amounts to a maximum perturbation of $\lceil 255 \cdot d \rceil$ bits across all pixels on the raw image.

As an alternative metric, we also plot the success rate at various distance thresholds for both algorithms given a limited budget of model queries. An adversarial example is defined a success if the size of perturbation does not exceed a given distance
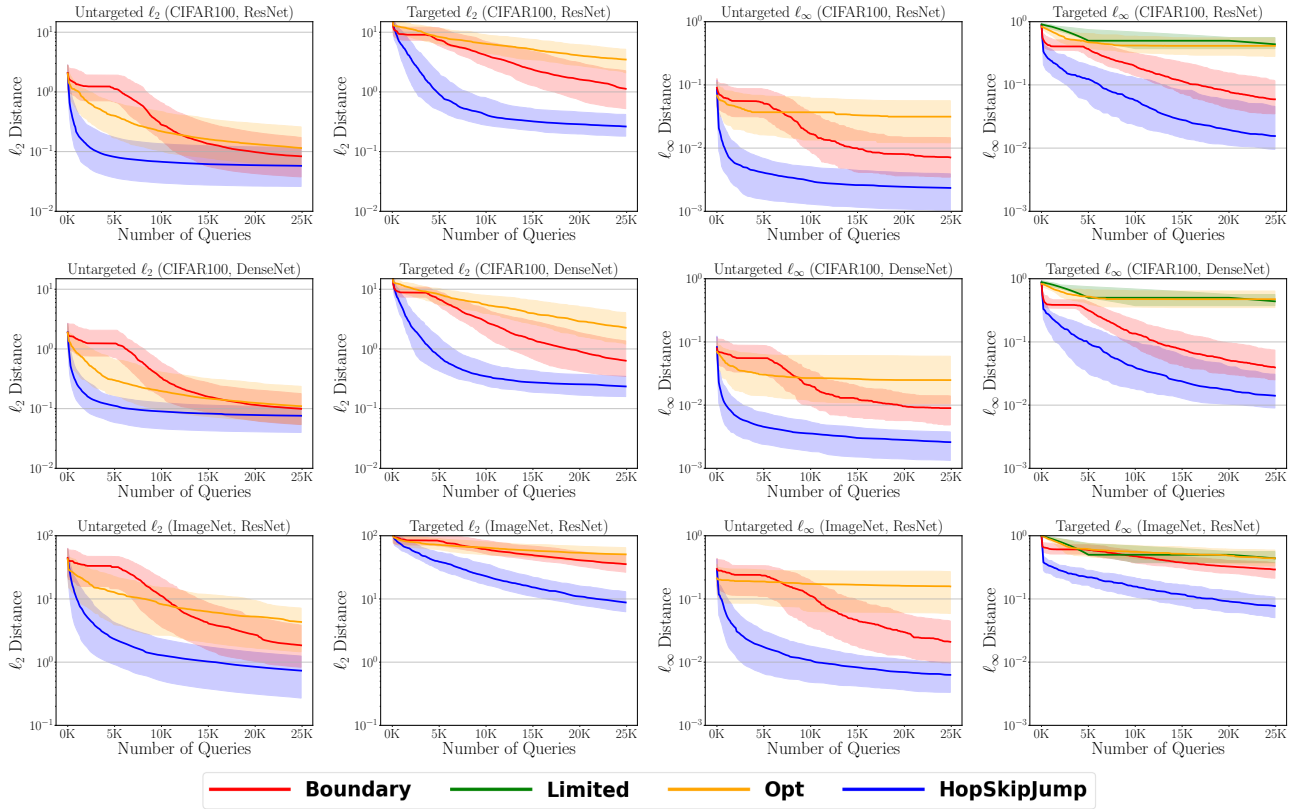
Figure 4. Median distance versus number of model queries on CIFAR-100 with ResNet, DenseNet, and ImageNet with ResNet from top to bottom rows. 1st column: untargeted ℓ_2. 2nd col.: targeted ℓ_2. 3rd col.: untargeted ℓ_∞. 4th col.: targeted ℓ_∞.

threshold. The success rate can be directly related to the accuracy of a model on perturbed data under a given distance threshold:

$$\text{perturbed acc.} = \text{original acc.} \times (1 - \text{success rate}). \tag{17}$$

Throughout the experiments, we limit the maximum budget of queries per image to 25,000, the setting of practical interest, due to limited computational resources.

Results   Figure 3 and 4 show the median distance (on a log scale) against the queries, with the first and third quartiles used as lower and upper error bars. For Boundary, Opt and HopSkipJumpAttack, Table 1 summarizes the median distance when the number of queries is fixed at 1,000, 5,000, and 20,000 across all distance types, data, models and objectives. Figure 5 and 6 show the success rate against the distance threshold. Figure 3 and 5 contain results on MNIST with CNN, and CIFAR-10 with ResNet, Denset, subsequently from the top row to the bottom row. Figure 4 and 6 contain results on CIFAR-100 with ResNet and DenseNet, and ImageNet with ResNet, subsequently from the top row to the bottom row. The four columns are for untargeted ℓ_2, targeted ℓ_2, untargeted ℓ_∞ and targeted ℓ_∞ attacks respectively.

With a limited number of queries, HopSkipJumpAttack is able to craft adversarial examples of a significantly smaller distance with the corresponding original examples across all data sets, followed by Boundary Attack and Opt Attack. As a concrete example, Table 1 shows that untargeted ℓ_2-optimized HopSkipJumpAttack achieves a median distance of 0.559 on CIFAR-10 with a ResNet model at $1,000$ queries, which amounts to below $3/255$ per pixel on average. At the same budget of queries, Boundary Attack and Opt Attack only achieve median ℓ_2-distances of 2.78 and 2.07 respectively. The difference in efficiency becomes more significant for ℓ_∞ attacks. As shown in Figure 5, under an untargeted ℓ_∞-optimized HopSkipJumpAttack with $1,000$ queries, all pixels are within an $8/255$-neighborhood of the original image for around 70% of adversarial examples, a
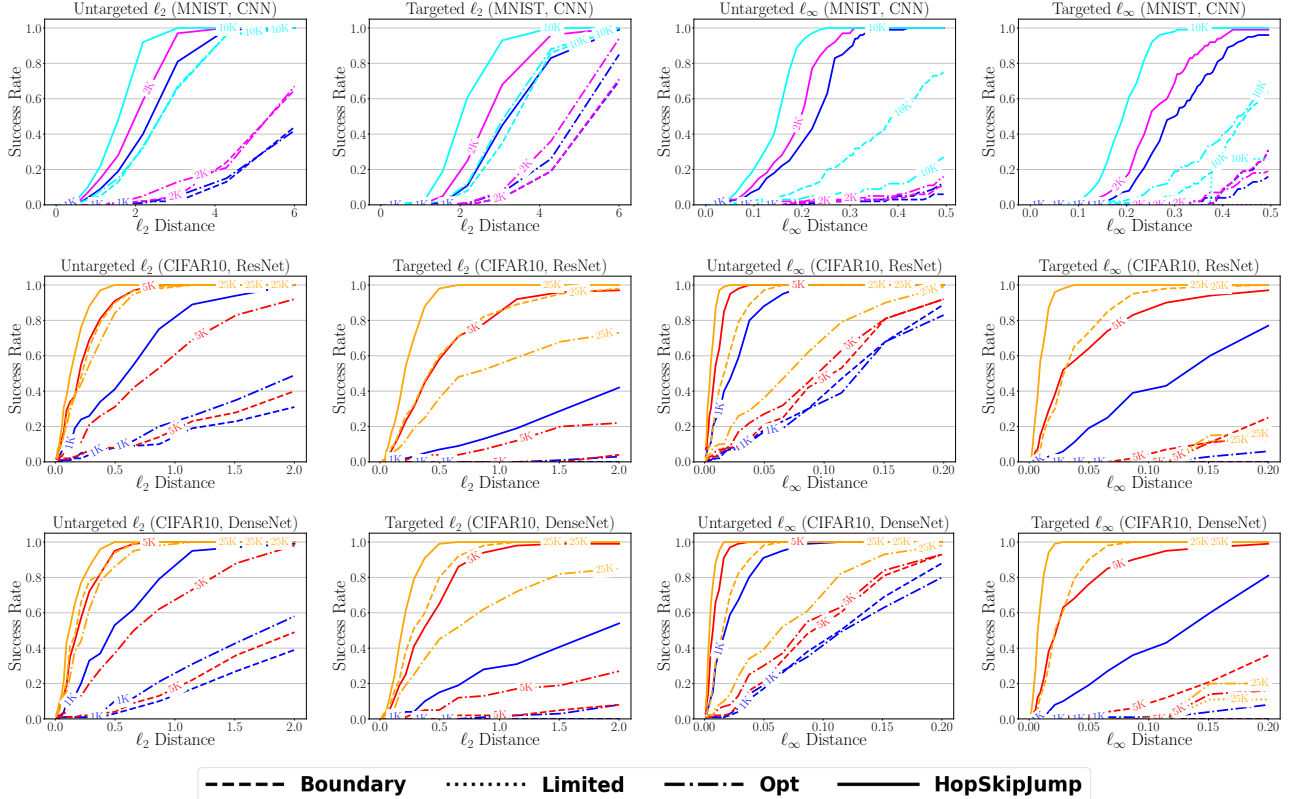
Figure 5. Success rate versus distance threshold for MNIST with CNN, and CIFAR-10 with ResNet, DenseNet from top to bottom rows. 1st column: untargeted ℓ_2. 2nd column: targeted ℓ_2. 3rd column: untargeted ℓ_∞. 4th column: targeted ℓ_∞.

success rate achieved by Boundary Attack only after 20,000 queries.

By comparing the odd and even columns of Figure 3-6, we can find that targeted HopSkipJumpAttack takes more queries than the untargeted one to achieve a comparable distance. This phenomenon becomes more explicit on CIFAR-100 and ImageNet, which have more classes. With the same number of queries, there is an order-of-magnitude difference in median distance between untargeted and targeted attacks (Figure 3 and 4). For ℓ_2-optimized HopSkipJumpAttack, while the untargeted version is able to craft adversarial images by perturbing 4 bits per pixel on average within 1,000 queries for $70\% - 90\%$ of images in CIFAR-10 and CIFAR-100, the targeted counterpart takes 2,000-5,000 queries. The other attacks fail to achieve a comparable performance even with 25,000 queries. On ImageNet, untargeted ℓ_2-optimized HopSkipJumpAttack is able to fool the model with a perturbation of size 6 bits per pixel on average for close to 50% of images with $1,000$ queries; untargeted ℓ_∞-optimized HopSkipJumpAttack controls the maximum perturbation across all pixels within 16 bits for 50% images within $1,000$ queries. The targeted Boundary Attack is not able to control the perturbation size to such a small scale until after around $25,000$ queries. On the one hand, the larger query budget requirement results from a strictly more powerful formulation of targeted attack than untargeted attack. On the other hand, this is also because we initialize targeted HopSkipJumpAttack from an arbitrary image in the target class. The algorithm may be trapped in a bad local minimum with such an initialization. Future work can address systematic approaches to better initialization.

As a comparison between data sets and models, we see that adversarial images often have a larger distance to their corresponding original images on MNIST than on CIFAR-10 and CIFAR-100, which has also been observed in previous work (e.g., [6]). This might be because it is more difficult to fool a model on simpler tasks. On the other hand, HopSkipJumpAttack also converges in a fewer number of queries on MNIST, as is shown in Figure 3. It does not converge even after $25,000$ queries on ImageNet. We conjecture the query budget is related to the input dimension, and the smoothness of decision boundary. We also observe the difference in model structure does not have a large influence on decision-based algorithms, if the training
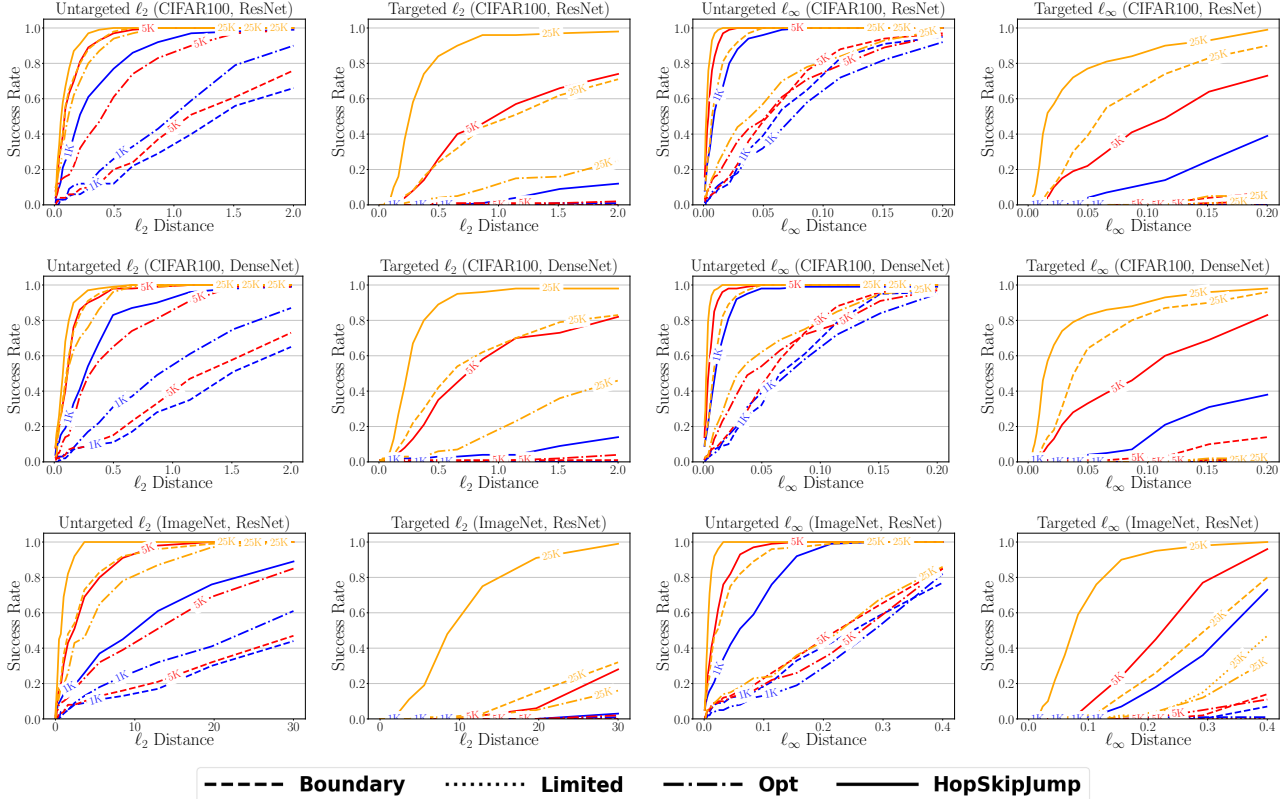
Figure 6. Success rate versus distance threshold for CIFAR-100 with ResNet, DenseNet, and ImageNet with ResNet from top to bottom rows. 1st column: untargeted ℓ_2. 2nd column: targeted ℓ_2. 3rd column: untargeted ℓ_∞. 4th column: targeted ℓ_∞.

algorithm and the data set keep the same. For ResNet and DenseNet trained on a common data set, a decision-based algorithm achieves comparable performance in crafting adversarial examples, although DenseNet has a more complex structure than ResNet.

As a comparison with state-of-the-art white-box targeted attacks, C&W attack [6] achieves an average ℓ_2-distance of 0.33 on CIFAR-10, and BIM [3] achieves an average ℓ_∞-distance of 0.014 on CIFAR-10. Targeted HopSkipJumpAttack achieves a comparable distance with 5K-10K model queries on CIFAR-10, without access to model details. On ImageNet, targeted C&W attack and BIM achieve an ℓ_2-distance of 0.96 and an ℓ_∞-distance of 0.01 respectively. Untargeted HopSkipJumpAttack achieves a comparable performance with $10,000 - 15,000$ queries. The targeted version is not able to perform comparably as targeted white-box attacks when the budget of queries is limited within $25,000$.

Visualized trajectories of HopSkipJumpAttack optimized for ℓ_2 distances along varied queries on CIFAR10 and ImageNet can be found in Figure 7. On CIFAR-10, we observe untargeted adversarial examples can be crafted within around 500 queries; targeted HopSkipJumpAttack is capable of crafting human indistinguishable targeted adversarial examples within around $1,000 - 2,000$ queries. On ImageNet, untargeted HopSkipJumpAttack is able to craft good adversarial examples with $1,000$ queries, while targeted HopSkipJumpAttack takes $10,000 - 20,000$ queries.

5.2 Defense mechanisms under decision-based attacks

We investigate the robustness of various defense mechanisms under decision-based attacks.

Figure 7. Visualized trajectories of HopSkipJumpAttack for optimizing ℓ_2 distance on randomly selected images in CIFAR-10 and ImageNet. 1st column: initialization (after blended with original images). 2nd-9th columns: images at 100, 200, 500, 1K, 2K, 5K, 10K, 25K model queries. 10th column: original images.

Defense mechanisms   Three defense mechanisms are evaluated: defensive distillation, region-based classification, and adversarial training. Defensive distillation [33], a form of gradient masking [13], trains a second model to predict the output probabilities of an existing model of the same structure. We use the implementaion provided by Carlini and Wagner [6] for defensive distillation. The second defense, region-based classification, belongs to a wide family of mechanisms which add test-time randomness to the inputs or the model, causing the gradients to be randomized [34]. Multiple variants have been proposed to randomize the gradients [35–39]. We adopt the implementation in Cao and Gong [35] with suggested noise levels. Given a trained base model, region-based classification samples points from the hypercube centered at the input image, predicts the label for each sampled point with the base model, and then takes a majority vote to output the label. Adversarial training [2, 3, 7, 17] is known to be one of the most effective defense mechanisms against adversarial perturbation [40, 34]. We evaluate a publicly available model trained through a robust optimization method proposed by Madry et al. [7]. We further evaluate our attack method by constructing a non-differentiable model via input binarization followed by a random forest in Section 5.3. The evaluation is carried out on MNIST, where defense mechanisms such as adversarial training work most effectively.

Baselines   We compare our algorithm with state-of-the-art attack algorithms that require access to gradients, including C&W Attack [6], DeepFool [4] for minimizing ℓ_2-distance, and FGSM [2], and BIM [41, 7] for minimizing ℓ_∞-distance. For region-based classification, the gradient of the base classifier is taken with respect to the original input.

We further include methods designed specifically for the defense mechanisms under threat. For defensive distillation, we include the ℓ_∞-optimized C&W Attack [6]. For region-based classification, we include backward pass differentiable approximation (BPDA) [34], which calculates the gradient of the model at a randomized input to replace the gradient at the original input in C&W Attack and BIM. All of these methods assume access to model details or even defense mechanisms, which is a stronger threat model than the one required for decision-based attacks. We also include Boundary Attack as a decision-based baseline.

For HopSkipJumpAttack and Boundary Attack, we include the success rate at three different scales of query budget: 2K, 10K and 50K, so as to evaluate our method both with limited queries and a sufficient number of queries. We find the convergence of
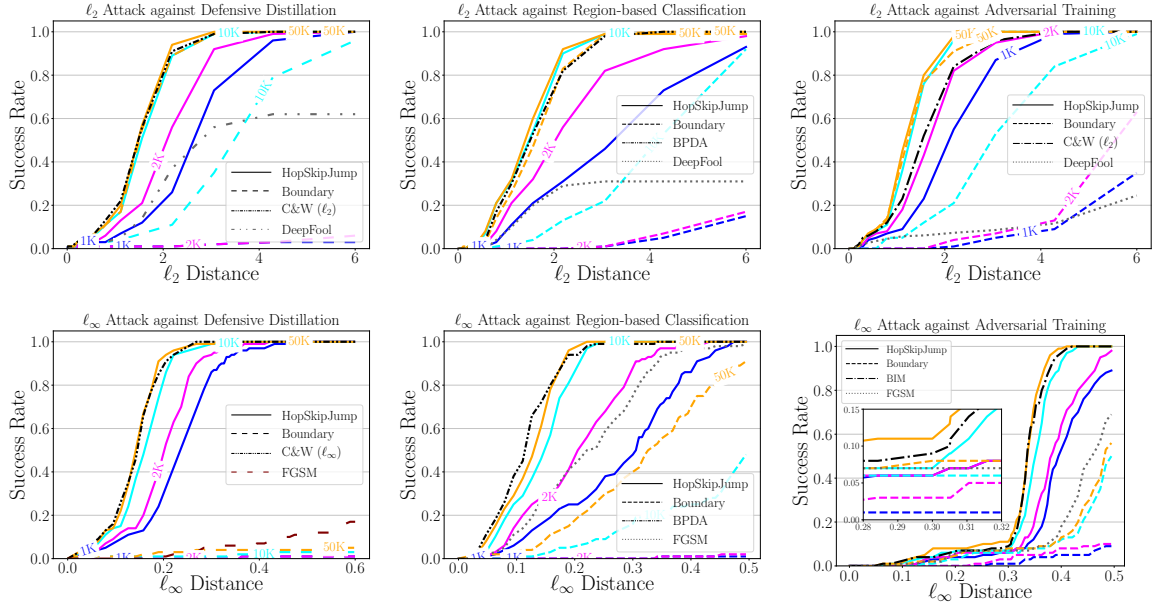
Figure 8. Success rate versus distance threshold for a distilled model, a region-based classifier and an adversarially trained model on MNIST. Blue, magenta, cyan and orange lines are used for HopSkipJumpAttack and Boundary Attack at the budget of 1K, 2K, 10K and 50K respectively. Different attacks are plotted with different line styles. An amplified figure is included near the critical ℓ_∞-distance of 0.3 for adversarial training.

HopSkipJumpAttack becomes unstable on region-based classification, resulting from the difficulty of locating the boundary in the binary search step when uncertainty is increased near the boundary. Thus, we increase the binary search threshold to 0.01 to resolve this issue.

Results   Figure 8 shows the success rate of various attacks at different distance thresholds for the three defense mechanisms. On all of the three defenses, HopSkipJumpAttack demonstrates similar or superior performance compared to state-of-the-art white-box attacks with sufficient model queries. Even with only 1K-2K model queries, it also achieves acceptable performance, although worse than the best white-box attacks. With sufficient queries, Boundary Attack achieves a comparable performance under the ℓ_2-distance metric. But it is not able to generate any adversarial examples when the number of queries is limited to $1,000$. We think this is because the strength of our batch gradient direction estimate over the random walk step in Boundary Attack becomes more explicit when there is uncertainty or non-smoothness near the decision boundary. We also observe that Boundary Attack does not work in optimizing the ℓ_∞-distance metric for adversarial examples, making it difficult to evaluate defenses designed for ℓ_∞ distance, such as adversarial training proposed by Madry et al. [7].

On a distilled model, when the ℓ_∞-distance is thresholded at 0.3, a perturbation size proposed by Madry et al. [7] to measure adversarial robustness, HopSkipJumpAttack achieves success rates of 86% and 99% with 1K and 50K queries respectively. At an ℓ_2-distance of 3.0, the success rate is 91% with 2K queries. HopSkipJumpAttack achieves a comparable performance with C&W attack under both distance metrics with 10K-50K queries. Also, gradient masking [13] by defensive distillation does not have a large influence on the query efficiency of HopSkipJumpAttack, indicating that the gradient direction estimate is robust under the setting where the model does not have useful gradients for certain white-box attacks.

On region-based classification, with 2K queries, HopSkipJumpAttack achieves success rates of 82% and 93% at the same ℓ_∞- and ℓ_2-distance thresholds respectively. With 10K-50K queries, it is able to achieve a comparable performance to BPDA, a white-box attack tailored to such defense mechanisms. On the other hand, we observe that HopSkipJumpAttack converges slightly slower on region-based classification than itself on ordinary models, which is because stochasticity near the boundary may prevent binary search in HopSkipJumpAttack from locating the boundary accurately.
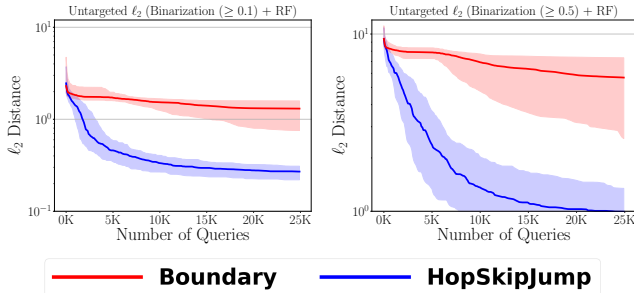
Figure 9. Median ℓ_2 distance versus number of model queries on MNIST with binarization + random forest. The threshold of binarization is set to be 0.1 and 0.5 respectively.
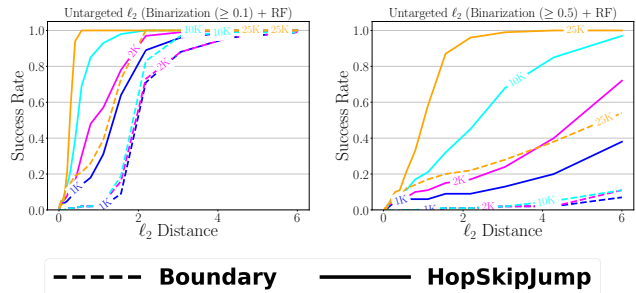
Figure 10. Success rate versus distance threshold on MNIST with binarization + random forest. The threshold of binarization is set to be 0.1 and 0.5 respectively.

On an adversarially trained model, HopSkipJumpAttack achieves a success rate of 11.0% with 50K queries when the ℓ_∞-distance is thresholded at 0.3. As a comparison, BIM has a success rate of 7.4% at the given distance threshold. The success rate of ℓ_∞-HopSkipJumpAttack transfers to an accuracy of 87.58% on adversarially perturbed data, close to the state-of-the-art performance achieved by white-box attacks.[4] With 1K queries, HopSkipJumpAttack also achieves comparable performance to BIM and C&W attack.

5.3 Model without gradients

In this section, we evaluate HopSkipJumpAttack on a model without gradients. We aim to show HopSkipJumpAttack is able to craft adversarial examples under weaker conditions, such as non-differentiable models, or even discontinuous input transform.

Concretely, we implement input binarization followed by a random forest on MNIST. Binarization transforms an input image to an array of $\{0, 1\}$, but transforming all pixels larger than a given threshold to 1, and all pixels smaller than the threshold to 0. The algorithm for training random forests applies bootstrap aggregating to tree learners. We implement the random forest with default parameters in scikit-learn [42], using the Gini impurity as split criterion. For each split, $\sqrt{d}$ randomly selected features are used, where $d = 28 \times 28$ is the number of pixels. We evaluate two random forests with different thresholds for binarization: 0.1 and 0.5. With the first threshold, the model achieves the highest accuracy, 96%, on natural test data. The second threshold yields the most robust performance under adversarial perturbation, with accuracy 94.5% on natural test data.

For both Boundary Attack and HopSkipJumpAttack, we adopt the same initialization and hyper-parameters as in Section 5.1. The original image (with real values) is used as input to both attacks for model queries. When an image is fed into the model by the attacker, the model processes the image with binarization first, followed by the random forest. Such a design preserves the black-box assumption for decision-based attacks. We only focus on untargeted ℓ_2 attack here. Note that over 91% of the pixels on MNIST are either greater than 0.9 or less than 0.1, and thus require a perturbation of size at least 0.4 to change their outputs after being thresholded by 0.5. This fact makes ℓ_∞ perturbation inappropriate for crafting adversarial examples.

Figure 9 shows the median distance (on a log scale) against the queries, with the first and third quartiles used as lower and upper error bars. Figure 10 shows the success rate against the distance threshold. When the threshold is set to be 0.1, the random forest with binarization becomes extremely vulnerable to adversarial examples. Around 96% adversarial examples fall into the size-3 ℓ_2-neighborhood of the respective original examples with 1K model queries of HopSkipJumpAttack. The vulnerability is caused by the ease of activating pixels through increasing the strength by 0.1. It also indicates HopSkipJumpAttack and Boundary Attack are able to craft adversarial examples without smooth decision boundaries.

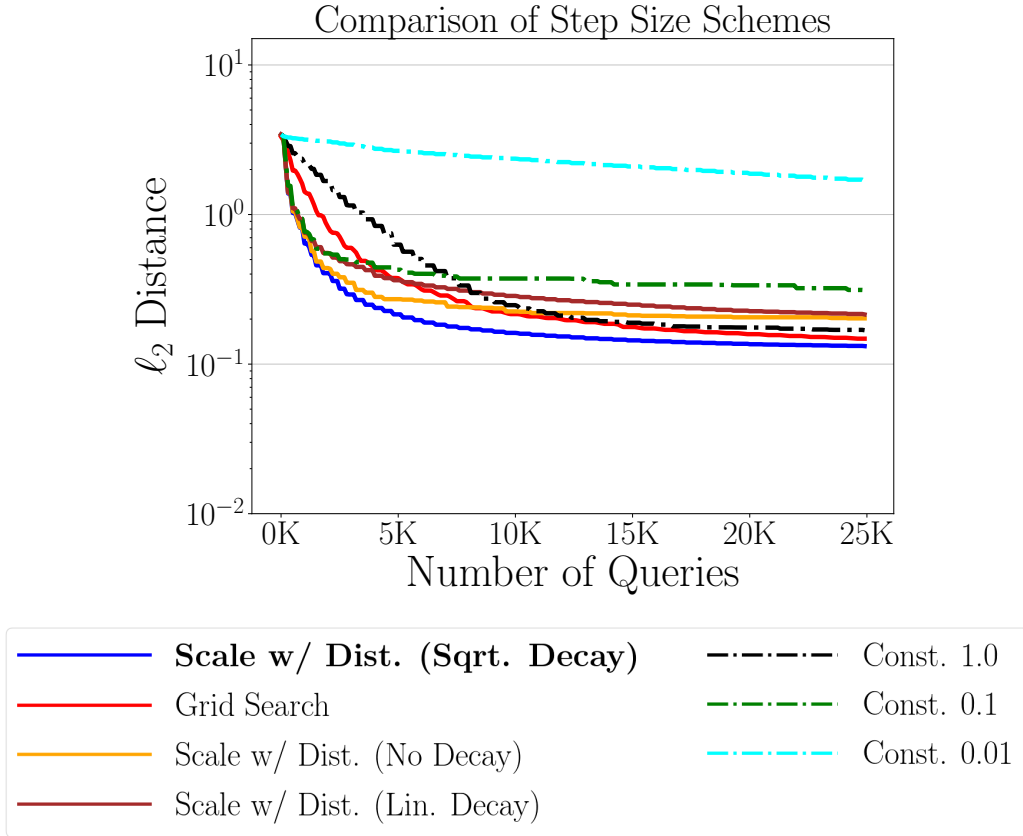[4]See https://github.com/MadryLab/mnist_challenge

Figure 11: Comparison of various choices of step size.

When the threshold is set to be 0.5, we have a more robust model. A median $\ell_2$distance of 3 is achieved by HopSkipJumpAttack through 3K model queries. It takes 25K queries to achieve 99% success rate at an ℓ_2 distance of 3 for HopSkipJumpAttack. On the other hand, we observe that Boundary Attack only achieves a median distance of 5 even with 25K model queries. This might result from the inefficiency in spending queries on random walk instead of "gradient direction" estimation step in HopSkipJumpAttack. We remark that the concept of "gradient direction" requires an alternative definition in the current setting, such as a formulation via subgradients.

5.4 Sensitivity analysis

In this section, we carry out experiments to evaluate the hyper-parameters suggested by our theoretical analysis. We use a 20-layer ResNet [31] trained over CIFAR-10 [27]. We run the ℓ_2-optimized HopSkipJumpAttack over a subset of randomly sampled images.

Choice of step size   We compare several schemes of choosing step size at each step. The first scheme is suggested by Theorem 1: at the t-th step, we set $\xi_t = \|x_t - x^\star\|_2/\sqrt{t}$, which we call "Scale with Distance (Sqrt. Decay)." We include the other two scales which scale with distance, "Scale with Distance (Linear Decay)" with $\xi_t = \|x_t - x^\star\|_2/t$ and "Scale with Distance (No Decay)" with $\xi_t = \|x_t - x^\star\|_2$. We then include "Grid Search," which searchs step sizes over a log-scale grid, and chooses the step size that best controls the distance with the original sample after projecting the updated sample back to the boundary via binary search. Finally, we include constant stepsizes at $\xi_t = 0.01, 0.1, 1.0$. For all schemes, we always use
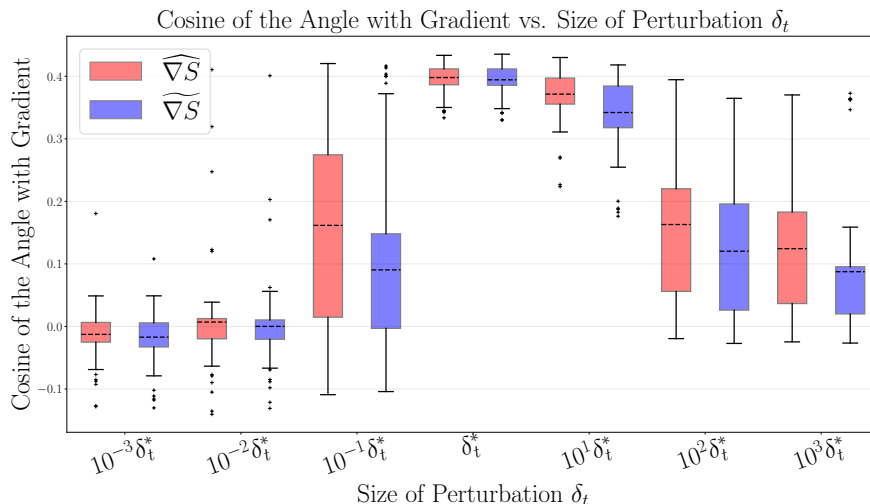
Figure 12: Box plots of the cosine of the angle between the proposed estimates and the true gradient.

geometric progression to decrease the step size by half until $\phi_{x^\star}(\tilde{x}_t) = 1$ before the next binary search step.

Figure 11 plots the median distance against the number of queries for all schemes. We observe that the scheme suggested by Theorem 1 achieves the best performance in this experiment. Grid search costs extra query budget initially but eventually achieves a comparable convergence rate. When the step size scales with the distance but with inappropriately chosen decay, the algorithm converges slightly slower. The performance of the algorithm suffers from a constant step size.

Choice of perturbation size and introduction of baseline   We now study the effectiveness of the proposed perturbation size and baseline for estimating gradient direction when the sample deviates from the boundary. In particular, we focus on the choice of δ_t and the introduction of baseline analyzed in Section 4. Gradient direction estimation is carried out at perturbed images at the ith iteration, for $i = 10, 20, 30, 40, 50, 60$. We use the cosine of the angle between the gradient-direction estimate and the truth gradient of the model as a metric.

Figure 12 shows the box plots of two gradient-direction estimates as δ_t varies among $0.01\delta_t^*, 0.1\delta_t^*, \delta_t^*, 10\delta_t^*, 100\delta_t^*$, where $\delta_t^* = 10\sqrt{d}\theta\|\tilde{x}_{t-1} - x^\star\|_2$ is our proposed choice. We observe that our proposed choice of δ_t yields the highest cosine of the angle on average. Also, the baseline in $\widehat{\nabla S}$ further improves the performance, in particular when δ_t is not chosen optimally so that there is severe unevenness in the distribution of perturbed images.

6   Discussion

We have proposed a family of query-efficient algorithms based on a novel gradient-direction estimate, HopSkipJumpAttack, for decision-based generation of adversarial examples, which is capable of optimizing ℓ_2 and ℓ_∞-distances for both targeted and untargeted attacks. Convergence analysis has been carried out given access to the gradient. We have also provided analysis for the error of our Monte Carlo estimate of gradient direction, which comes from three sources: bias at the boundary for a nonzero perturbation size, bias of deviation from the boundary, and variance. Theoretical analysis has provided insights for selecting the step size and the perturbation size, which leads to a hyperparameter-free algorithm. We have also carried out extensive experiments, showing HopSkipJumpAttack compares favorably to Boundary Attack in query efficiency, and

achieves competitive performance on several defense mechanisms.

Given the fact that HopSkipJumpAttack is able to craft a human-indistinguishable adversarial example within a realistic budget of queries, it becomes important for the community to consider the real-world impact of decision-based threat models. We have also demonstrated that HopSkipJumpAttack is able to achieve comparable or even superior performance to state-of-the-art white-box attacks on several defense mechanisms, under a much weaker threat model. In particular, masked gradients, stochastic gradients, and non-differentiability are not barriers to our algorithm. Because of its effectiveness, efficiency, and applicability to non-differentiable models, we suggest future research on adversarial defenses may evaluate the designed mechanism against HopSkipJumpAttack as a first step.

One limitation of all existing decision-based algorithms, including HopSkipJumpAttack, is that they require evaluation of the target model near the boundary. They may not work effectively by limiting the queries near the boundary. We have also observed that it still takes tens of thousands of model queries for HopSkipJumpAttack to craft imperceptible adversarial examples with a target class on ImageNet, which has a relatively large image size. Future work may seek the combination of HopSkipJumpAttack with transferred attack to resolve these issues.

References

[1] Christian Szegedy, Wojciech Zaremba, Ilya Sutskever, Joan Bruna, Dumitru Erhan, Ian Goodfellow, and Rob Fergus. Intriguing properties of neural networks. In *International Conference on Learning Representations*, 2014.

[2] Ian J Goodfellow, Jonathon Shlens, and Christian Szegedy. Explaining and harnessing adversarial examples. In *Proceedings of the International Conference on Learning Representations*, 2015.

[3] Alexey Kurakin, Ian Goodfellow, and Samy Bengio. Adversarial machine learning at scale. In *International Conference on Learning Representations*, 2017.

[4] Seyed-Mohsen Moosavi-Dezfooli, Alhussein Fawzi, and Pascal Frossard. Deepfool: a simple and accurate method to fool deep neural networks. In *Proceedings of the IEEE Conference on Computer Vision and Pattern Recognition*, pages 2574–2582, 2016.

[5] Nicolas Papernot, Patrick McDaniel, Somesh Jha, Matt Fredrikson, Z Berkay Celik, and Ananthram Swami. The limitations of deep learning in adversarial settings. In *2016 IEEE European Symposium on Security and Privacy*, pages 372–387. IEEE, 2016.

[6] Nicholas Carlini and David Wagner. Towards evaluating the robustness of neural networks. In *2017 IEEE Symposium on Security and Privacy*, pages 39–57. IEEE, 2017.

[7] Aleksander Madry, Aleksandar Makelov, Ludwig Schmidt, Dimitris Tsipras, and Adrian Vladu. Towards deep learning models resistant to adversarial attacks. In *International Conference on Learning Representations*, 2018.

[8] Pin-Yu Chen, Huan Zhang, Yash Sharma, Jinfeng Yi, and Cho-Jui Hsieh. Zoo: Zeroth order optimization based black-box attacks to deep neural networks without training substitute models. In *Proceedings of the 10th ACM Workshop on Artificial Intelligence and Security*, pages 15–26. ACM, 2017.

[9] Andrew Ilyas, Logan Engstrom, Anish Athalye, and Jessy Lin. Black-box adversarial attacks with limited queries and information. In *International Conference on Machine Learning*, pages 2142–2151, 2018.

[10] Andrew Ilyas, Logan Engstrom, and Aleksander Madry. Prior convictions: Black-box adversarial attacks with bandits and priors. In *International Conference on Learning Representations*, 2019.

[11] Yanpei Liu, Xinyun Chen, Chang Liu, and Dawn Song. Delving into transferable adversarial examples and black-box attacks. In *Proceedings of the International Conference on Learning Representations*, 2017.

[12] Nicolas Papernot, Patrick McDaniel, and Ian Goodfellow. Transferability in machine learning: from phenomena to black-box attacks using adversarial samples. *arXiv preprint arXiv:1605.07277*, 2016.

[13] Nicolas Papernot, Patrick McDaniel, Ian Goodfellow, Somesh Jha, Z Berkay Celik, and Ananthram Swami. Practical black-box attacks against machine learning. In *Proceedings of the 2017 ACM on Asia Conference on Computer and Communications Security*, pages 506–519. ACM, 2017.

[14] Wieland Brendel, Jonas Rauber, and Matthias Bethge. Decision-based adversarial attacks: Reliable attacks against black-box machine learning models. In *International Conference on Learning Representations*, 2018.

[15] Thomas Brunner, Frederik Diehl, Michael Truong Le, and Alois Knoll. Guessing smart: Biased sampling for efficient black-box adversarial attacks. *arXiv preprint arXiv:1812.09803*, 2018.

[16] Minhao Cheng, Thong Le, Pin-Yu Chen, Huan Zhang, JinFeng Yi, and Cho-Jui Hsieh. Query-efficient hard-label black-box attack: An optimization-based approach. In *International Conference on Learning Representations*, 2019.

[17] Florian Tramèr, Alexey Kurakin, Nicolas Papernot, Ian Goodfellow, Dan Boneh, and Patrick McDaniel. Ensemble adversarial training: Attacks and defenses. In *International Conference on Learning Representations*, 2018.

[18] Abraham D Flaxman, Adam Tauman Kalai, and H Brendan McMahan. Online convex optimization in the bandit setting: gradient descent without a gradient. In *Proceedings of the Sixteenth Annual ACM-SIAM Symposium on Discrete Algorithms*, pages 385–394. SIAM, 2005.

[19] Alekh Agarwal, Dean P Foster, Daniel J Hsu, Sham M Kakade, and Alexander Rakhlin. Stochastic convex optimization with bandit feedback. In *Advances in Neural Information Processing Systems*, pages 1035–1043, 2011.

[20] Yurii Nesterov and Vladimir Spokoiny. Random gradient-free minimization of convex functions. *Foundations of Computational Mathematics*, 17(2):527–566, 2017.

[21] John C Duchi, Michael I Jordan, Martin J Wainwright, and Andre Wibisono. Optimal rates for zero-order convex optimization: The power of two function evaluations. *IEEE Transactions on Information Theory*, 61(5):2788–2806, 2015.

[22] Sijia Liu, Bhavya Kailkhura, Pin-Yu Chen, Paishun Ting, Shiyu Chang, and Lisa Amini. Zeroth-order stochastic variance reduction for nonconvex optimization. In *Advances in Neural Information Processing Systems*, pages 3731–3741, 2018.

[23] David Kincaid, David Ronald Kincaid, and Elliott Ward Cheney. *Numerical Analysis: Mathematics of Scientific Computing*, volume 2. American Mathematical Soc., 2009.

[24] Michel Ledoux. *The Concentration of Measure Phenomenon*. Number 89. American Mathematical Soc., 2001.

[25] Nicolas Papernot, Fartash Faghri, Nicholas Carlini, Ian Goodfellow, Reuben Feinman, Alexey Kurakin, Cihang Xie, Yash Sharma, Tom Brown, Aurko Roy, Alexander Matyasko, Vahid Behzadan, Karen Hambardzumyan, Zhishuai Zhang, Yi-Lin Juang, Zhi Li, Ryan Sheatsley, Abhibhav Garg, Jonathan Uesato, Willi Gierke, Yinpeng Dong, David Berthelot, Paul Hendricks, Jonas Rauber, and Rujun Long. Technical report on the cleverhans v2.1.0 adversarial examples library. *arXiv preprint arXiv:1610.00768*, 2018.

[26] Jonas Rauber, Wieland Brendel, and Matthias Bethge. Foolbox: A python toolbox to benchmark the robustness of machine learning models. *arXiv preprint arXiv:1707.04131*, 2017.

[27] Alex Krizhevsky. Learning multiple layers of features from tiny images. Technical report, Citeseer, 2009.

[28] J. Deng, W. Dong, R. Socher, L.-J. Li, K. Li, and L. Fei-Fei. ImageNet: A Large-Scale Hierarchical Image Database. In *Proceedings of the IEEE Conference on Computer Vision and Pattern Recognition*, 2009.

[29] François Chollet et al. Keras. `https://keras.io`, 2015.

[30] Jan Hendrik Metzen, Tim Genewein, Volker Fischer, and Bastian Bischoff. On detecting adversarial perturbations. In *International Conference on Learning Representations*, 2017.

[31] Kaiming He, Xiangyu Zhang, Shaoqing Ren, and Jian Sun. Identity mappings in deep residual networks. In *European Conference on Computer Vision*, pages 630–645. Springer, 2016.

[32] Gao Huang, Zhuang Liu, Laurens Van Der Maaten, and Kilian Q Weinberger. Densely connected convolutional networks. In *Proceedings of the IEEE Conference on Computer Vision and Pattern Recognition*, pages 4700–4708, 2017.

[33] Nicolas Papernot, Patrick McDaniel, Xi Wu, Somesh Jha, and Ananthram Swami. Distillation as a defense to adversarial perturbations against deep neural networks. In *2016 IEEE Symposium on Security and Privacy*, pages 582–597. IEEE, 2016.

[34] Anish Athalye, Nicholas Carlini, and David Wagner. Obfuscated gradients give a false sense of security: Circumventing defenses to adversarial examples. In *International Conference on Machine Learning*, pages 274–283, 2018.

[35] Xiaoyu Cao and Neil Zhenqiang Gong. Mitigating evasion attacks to deep neural networks via region-based classification. In *Proceedings of the 33rd Annual Computer Security Applications Conference*, pages 278–287. ACM, 2017.

[36] Xuanqing Liu, Minhao Cheng, Huan Zhang, and Cho-Jui Hsieh. Towards robust neural networks via random self-ensemble. In *Proceedings of the European Conference on Computer Vision (ECCV)*, pages 369–385, 2018.

[37] Guneet S. Dhillon, Kamyar Azizzadenesheli, Jeremy D. Bernstein, Jean Kossaifi, Aran Khanna, Zachary C. Lipton, and Animashree Anandkumar. Stochastic activation pruning for robust adversarial defense. In *International Conference on Learning Representations*, 2018.

[38] Jeremy Cohen, Elan Rosenfeld, and Zico Kolter. Certified adversarial robustness via randomized smoothing. In *International Conference on Machine Learning*, pages 1310–1320, 2019.

[39] Cihang Xie, Jianyu Wang, Zhishuai Zhang, Zhou Ren, and Alan Yuille. Mitigating adversarial effects through randomization. In *International Conference on Learning Representations*, 2018.

[40] Nicholas Carlini and David Wagner. Adversarial examples are not easily detected: Bypassing ten detection methods. In *Proceedings of the 10th ACM Workshop on Artificial Intelligence and Security*, pages 3–14. ACM, 2017.

[41] Alexey Kurakin, Ian J Goodfellow, and Samy Bengio. Adversarial examples in the physical world. In *Artificial Intelligence Safety and Security*, pages 99–112. Chapman and Hall/CRC, 2018.

[42] F. Pedregosa, G. Varoquaux, A. Gramfort, V. Michel, B. Thirion, O. Grisel, M. Blondel, P. Prettenhofer, R. Weiss, V. Dubourg, J. Vanderplas, A. Passos, D. Cournapeau, M. Brucher, M. Perrot, and E. Duchesnay. Scikit-learn: Machine learning in Python. *Journal of Machine Learning Research*, 12:2825–2830, 2011.

[43] Jan A Snyman. *Practical Mathematical Optimization*. Springer, 2005.

A Proofs

For notational simplicity, we use the shorthand $S \equiv S_{x^\star}$ throughout the proofs.

A.1 Proof of Theorem 1

For notational simplicity, let us denote $\tau_t := \xi_t / \|\nabla S(x_t)\|_2$, so that the update (3) at iterate t can be rewritten as

$$x_{t+1} = \alpha_t x^\star + (1 - \alpha_t)(x_t + \tau_t \nabla S(x_t)). \tag{18}$$

Recalling our step size choice $\xi_t = \eta_t \|x_t - x^\star\|$ with $\eta_t := t^{-q}$, we have $\tau_t = \eta_t \frac{\|x_t - x^\star\|}{\|\nabla S(x_t)\|}$.

The squared distance ratio is

$$\frac{\|x_{t+1} - x^\star\|_2^2}{\|x_t - x^\star\|_2^2} = \frac{\|(1-\alpha)(\tau_t \nabla S(x_t) + x_t - x^\star)\|_2^2}{\|x_t - x^\star\|_2^2}. \tag{19}$$

By a second-order Taylor series, we have

$$0 = \langle \nabla S(x_t),\, x_{t+1} - x_t \rangle + \frac{1}{2}(x_{t+1} - x_t)^T H_t (x_{t+1} - x_t), \tag{20}$$

where $H_t = \nabla^2 S(\beta x_{t+1} + (1 - \beta)x_t)$ for some $\beta \in [0, 1]$. Plugging equation (18) into equation (20) yields

$$\langle \nabla S(x_t),\, -\alpha v_t + \tau_t \nabla S(x_t) \rangle + \frac{1}{2}(-\alpha v_t + \tau_t \nabla S(x_t))^T H_t (-\alpha v_t + \tau_t \nabla S(x_t)) = 0, \tag{21}$$

where we define $v_t := x_t - x^\star + \tau_t \nabla S(x_t)$. This can be rewritten as a quadratic equation with respect to α:

$$v_t^T H_t v_t \alpha^2 - 2\nabla S(x_t)^T (I + \tau_t H_t) v_t \alpha + \nabla S(x_t)^T (\tau_t^2 H_t + 2\tau_t I)\nabla S(x_t) = 0. \tag{22}$$

Solving for α yields

$$\alpha = \frac{\nabla S(x_t)^T (\tau_t^2 H_t + 2\tau_t I)\nabla S(x_t)}{2\nabla S(x_t)^T (I + \tau_t H_t) v_t} \cdot \frac{2}{1 + \sqrt{1 - \frac{v_t^T H_t v_t \nabla S(x_t)^T (\tau_t^2 H_t + 2\tau_t I)\nabla S(x_t)}{(\nabla S(x_t)^T (I + \tau_t H_t) v_t)^2}}} \tag{23}$$

$$\geq \frac{\nabla S(x_t)^T (\tau_t^2 H_t + 2\tau_t I)\nabla S(x_t)}{2\nabla S(x_t)^T (I + \tau_t H_t) v_t}. \tag{24}$$

In order to simplify the notation, define $\nabla_t := \nabla S(x_t)$ and $d_t := x_t - x^\star$, which leads to

$$\alpha \geq \frac{\nabla_t^T (\frac{1}{2}\tau_t^2 H + \tau_t I)\nabla_t}{\nabla_t^T (I + \tau_t H)(d_t + \tau_t \nabla_t)}.$$

Hence, we have

$$
\begin{aligned}
(1 - \alpha)^2 &\leq \Big(1 - \frac{\nabla_t^T(\frac{1}{2}\tau_t^2 H_t + \tau_t I)\nabla_t}{\nabla_t^T(I + \tau_t H_t)(d_t + \tau_t \nabla_t)} \Big)^2 \\
&= \Big(\frac{\frac{1}{2}\tau_t^2 \nabla_t^T H_t \nabla_t + \nabla_t^T d_t + \tau_t \nabla_t^T H_t d_t}{\tau_t \nabla_t^T \nabla_t + \tau_t^2 \nabla_t^T H_t \nabla_t + \nabla_t^T d_t + \tau_t \nabla_t^T H_t d_t} \Big)^2 \\
&\leq \Big(\frac{\frac{1}{2}\tau_t^2 L\|\nabla_t\|^2 + \nabla_t^T d_t + \tau_t L\|d_t\|\|\nabla_t\|}{(\tau_t + \frac{1}{2}\tau_t^2 L)\|\nabla_t\|^2 + \nabla_t^T d_t + \tau_t L\|d_t\|\|\nabla_t\|} \Big)^2 \\
&= \Big(\frac{r_t + (\frac{1}{2}\eta_t^2 + \eta_t)L\frac{\|d_t\|_2}{\|\nabla_t\|_2}}{\eta_t + r_t + (\frac{1}{2}\eta_t^2 + \eta_t)L\frac{\|d_t\|_2}{\|\nabla_t\|_2}} \Big)^2 \\
&\leq \Big(\frac{r_t + \eta_t \cdot \frac{3}{2}L\frac{\|d_t\|_2}{\|\nabla_t\|_2}}{r_t + \eta_t \cdot (1 + \frac{3}{2}L\frac{\|d_t\|_2}{\|\nabla_t\|_2})} \Big)^2.
\end{aligned}
$$

where

$$
r_t = \frac{\langle x_t - x^\star, \nabla S(x_t) \rangle}{\|x_t - x^\star\|_2 \|\nabla S(x_t)\|_2} = \frac{\langle d_t, \nabla_t \rangle}{\|d_t\|_2 \|\nabla_t\|_2}. \tag{25}
$$

Let $\kappa_t := \frac{3}{2}L\frac{\|d_t\|_2}{\|\nabla_t\|_2}$. Then we have κ_t is bounded:

$$
\kappa_t \leq \frac{3}{2}L\frac{\|x_0 - x^\star\|_2}{c}. \tag{26}
$$

Equation (19) and the bound on $(1 - \alpha)^2$ yield

$$
\frac{\|x_{t+1} - x^\star\|_2^2}{\|x_t - x^\star\|_2^2} = (1 - \alpha)^2 \cdot \Big(\frac{\tau_t^2 \|\nabla S(x_t)\|^2 + 2\tau_t \langle \nabla S(x_t), x_t - x^\star \rangle}{\|x_t - x^\star\|^2} + 1 \Big) \tag{27}
$$

$$
= (1 - \alpha)^2 \cdot (\eta_t^2 + 2\eta_t r_t + 1) \tag{28}
$$

$$
\leq \Big(\frac{r_t + \eta_t \kappa_t}{r_t + \eta_t(1 + \kappa_t)} \Big)^2 \cdot (\eta_t^2 + 2\eta_t r_t + 1). \tag{29}
$$

We will show the convergence of r_t to 1 in two steps. In the first step, we show $\lambda_t := \frac{\eta_t}{r_t} \to 0$ by contradiction. In the second step, we establish the convergence rate of r_t to 1 based on the result of the first step.

Assume there exists a subsequence λ_{t_i} of λ_t that is bounded away from 0, such that $\lambda_{t_i} > c_1$ for some constant c_1. (Note that we always have $r_t > 0$ as x_t is on the target side of the boundary for any t.)

Define $\theta_t := \Big(\frac{r_t + \eta_t \kappa_t}{r_t + \eta_t(1 + \kappa_t)} \Big)^2 \cdot (\eta_t^2 + 2\eta_t r_t + 1)$. Then we have

$$
\theta_{t_i} \leq \Big(\frac{1 + c_1 \kappa_t}{1 + c_1(1 + \kappa_t)} \Big)^2 \cdot (\eta_{t_i}^2 + 2\eta_{t_i} + 1). \tag{30}
$$

As $\eta_{t_i} \to 0$, there exists a constant $c_2 > 0$ such that $\theta_{t_i} < 1 - c_2$ for i large enough.

Because θ_t is an increasing function of r_t, we have

$$
\theta_t \leq \Big(\frac{1 + \eta_t \kappa_t}{1 + \eta_t(1 + \kappa_t)} \Big)^2 \cdot (\eta_t^2 + 2\eta_t + 1) \tag{31}
$$

$$
= \frac{1 + 2\eta_t + 2\kappa_t \eta_t + \mathcal{O}(\eta_t^2)}{1 + 2\eta_t + 2\kappa_t \eta_t + \mathcal{O}(\eta_t^2)} \tag{32}
$$

$$
= 1 + \mathcal{O}(t^{-2q}). \tag{33}
$$

The product of $1 + t^{-2q}$ over t from 1 to ∞ is finite when $q > \frac{1}{4}$:

$$\Pi_{t=1}^{\infty}(1 + t^{-2q}) = \exp\{\sum_{t=1}^{\infty} \log(1 + t^{-2q})\} \tag{34}$$

$$\leq \exp\{\sum_{t=1}^{\infty} t^{-2q}\} < \infty. \tag{35}$$

Therefore, we have

$$\Pi_{t=1}^{\infty}\theta_t \leq \Pi_{i=1}^{\infty}\theta_{t_i} \cdot \Pi_{t=1}^{\infty}(1 + \mathcal{O}(t^{-2q})) = 0, \tag{36}$$

which implies x_t converges to $x^\star$, a contradiction. Therefore, $\lambda_t \to 0$ as $t \to \infty$.

Now we can establish the convergence of r_t to 1. We expand θ_t as

$$\theta_t = \frac{(1 + 2\lambda_t\kappa_t + \lambda_t^2\kappa_t^2)(\eta_t^2 + 2\eta_t r_t + 1)}{1 + 2\lambda_t(1 + \kappa_t) + \lambda_t^2(1 + \kappa_t)^2} \tag{37}$$

$$= \frac{1 + 2\lambda_t\kappa_t + \lambda_t^2\kappa_t^2 + 2\lambda_t r_t^2}{1 + 2\lambda_t\kappa_t + \lambda_t^2(\kappa_t + 1)^2 + 2\lambda_t} + \frac{\eta_t^2(4\kappa_t + (1 + \lambda_t\kappa_t)^2 + 2\lambda_t\kappa_t^2)}{1 + 2\lambda_t\kappa_t + \lambda_t^2(\kappa_t + 1)^2 + 2\lambda_t}$$

$$\leq \frac{1 + 2\lambda_t\kappa_t + \lambda_t^2\kappa_t^2 + 2\lambda_t r_t^2}{1 + 2\lambda_t\kappa_t + \lambda_t^2\kappa_t^2 + 2\lambda_t} + \eta_t^2(4\kappa_t + (1 + \lambda_t\kappa_t)^2 + 2\lambda_t\kappa_t^2)$$

$$\leq 1 - \frac{2\lambda_t(1 - r_t^2)}{1 + 2\lambda_t\kappa_t + \lambda_t^2\kappa_t^2 + 2\lambda_t} + \eta_t^2(4\kappa_t + 2) \tag{38}$$

$$\leq 1 - \lambda_t(1 - r_t^2) + \eta_t^2(4\kappa_t + 2), \tag{39}$$

where Inequality (38) holds for large enough t. As the product of θ_t over t is positive, we have

$$\sum_{t=1}^{\infty} \log\theta_t = \log\Pi_{t=1}^{\infty}\theta_t > -\infty. \tag{40}$$

Given that $\eta_t^2(4\kappa_t + 2) = \Theta(t^{-2q})$, Equation (40) is equivalent to

$$\sum_{t=1}^{\infty} \lambda_t(1 - r_t^2) < \infty, \tag{41}$$

which implies $\lambda_t(1 - r_t^2) = o(t^{-\frac{1}{2}})$.

As $r_t \leq 1$ and $\eta_t = t^{-q}$, we have $\lambda_t = \mathcal{O}(t^{-q})$ and hence we have $1 - r_t = o(t^{-\frac{1}{2}+q})$.

A.2 Proof of Theorem 2

The idea of the proof is to divide the unit sphere into three components: the upper cap along the direction of gradient, the lower cap opposite to the direction of gradient, and the annulus in between.

Let u be a random vector uniformly distributed on the sphere. By Taylor's theorem, for any $\delta \in (0, 1)$, we have

$$S(x_t + \delta u) = \delta\nabla S(x_t)^T u + \frac{1}{2}\delta^2 u^T \nabla^2 S(x')u. \tag{42}$$

for some x' on the line between x_t and $x_t + \delta u$, where we have made use of the fact that $S(x_t) = 0$. As the function S has Lipschitz gradients, we can bound the second-order term as

$$|\frac{1}{2}\delta^2 u^T \nabla^2 S(x')u| \leq \frac{1}{2}L\delta^2. \tag{43}$$

Let $w := \frac{1}{2}L\delta$. By the Taylor expansion and the bound on the second order term by eigenvalues, when $\nabla S(x_t)^T u > w$, we have

$$S(x_t + \delta u) \geq \delta \nabla S(x_t)^T u + \frac{1}{2}\delta^2 u^T \nabla^2 S(x')u$$

$$\geq \delta(\nabla S(x_t)^T u - \frac{1}{2}L\delta) > 0.$$

Similarly, we have $S(x_t + \delta u) < 0$ when $\nabla S(x_t)^T u < -w$. Therefore, we have

$$\phi_x(x_t + \delta u) = \begin{cases} 1 \text{ if } \nabla S(x_t)^T u > w, \\ -1 \text{ if } \nabla S(x_t)^T u < -w. \end{cases}$$

We expand the vector $\nabla S(x_t)$ to an orthogonal bases in $\mathbb{R}^d$: $v_1 = \nabla S(x_t)/\|\nabla S(x_t)\|_2, v_2, \ldots, v_d$. The random vector u can be expressed as

$$u = \sum_{i=1}^{d} \beta_i v_i,$$

where β is uniformly distributed on the sphere. Denote the upper cap as $E_1 := \{\nabla S(x_t)^T u > w\}$, the annulus as $E_2 := \{|\nabla S(x_t)^T u| < w\}$, and the lower cap as $E_3 := \{\nabla S(x_t)^T u < -w\}$. Let $p := \mathbb{P}(E_2)$ be the probability of event E_2. Thus we have $\mathbb{P}(E_1) = \mathbb{P}(E_3) = (1-p)/2$. By symmetry, for any $i \neq 1$, we have

$$\mathbb{E}[\beta_i \mid E_1] = \mathbb{E}[\beta_i \mid E_3] = 0.$$

Therefore, the expected value of the estimator is

$$\mathbb{E}[\phi_x(x_t + \delta u)u] = \left(\mathbb{E}[\phi_x(x_t + \delta u)u \mid E_1] + \mathbb{E}[\phi_x(x_t + \delta u)u \mid E_3]\right) \cdot (1-p)/2 + \mathbb{E}[\phi_x(x_t + \delta u)u \mid E_2] \cdot p$$

$$= \left(\mathbb{E}[\sum_{i=1}^{d} \beta_i v_i \mid E_1] + \mathbb{E}[-\sum_{i=1}^{d} \beta_i v_i \mid E_3]\right) \cdot (1-p)/2 + \mathbb{E}[\phi_x(x_t + \delta u)u \mid E_2] \cdot p$$

$$= \left(\mathbb{E}[\beta_1 v_1 \mid E_1] + \mathbb{E}[-\beta_1 v_1 \mid E_3]\right) \cdot (1-p)/2 + \mathbb{E}[\phi_x(x_t + \delta u)u \mid E_2] \cdot p$$

$$= p \cdot \left(\mathbb{E}[\phi_x(x_t + \delta u)u \mid E_2] - \frac{1}{2}\mathbb{E}[\beta_1 v_1 \mid E_1] - \frac{1}{2}\mathbb{E}[-\beta_1 v_1 \mid E_3]\right) + \mathbb{E}[\beta_1 v_1 \mid E_1] + \mathbb{E}[-\beta_1 v_1 \mid E_3]$$

Exploiting the above derivation, we bound the difference between $\mathbb{E}[|\beta_1|v_1] = \frac{\mathbb{E}|\beta_1|}{\|\nabla S(x_t)\|_2}\nabla S(x_t)$ and $\mathbb{E}[\phi_x(x_t + \delta u)u]$. In fact, we have

$$\|\mathbb{E}[\phi_x(x_t + \delta u)u] - \mathbb{E}[|\beta_1|v_1]\|_2 \leq p\left\|\mathbb{E}[\phi_x(x_t + \delta u)u \mid E_2] - \frac{1}{2}\mathbb{E}[\beta_1 v_1 \mid E_1] - \frac{1}{2}\mathbb{E}[-\beta_1 v_1 \mid E_3]\right\|_2 +$$

$$\left\|\mathbb{E}[|\beta_1|v_1 \mid E_1] + \mathbb{E}[|\beta_1|v_1 \mid E_3] - \mathbb{E}[|\beta_1|v_1]\right\|_2$$

$$\leq 2p + p = 3p,$$

which yields

$$\cos \angle (\mathbb{E}[\phi_x(x_t + \delta u)u], \nabla S(x_t)) \geq 1 - \frac{1}{2}\left(\frac{3p}{\mathbb{E}|\beta_1|}\right)^2. \tag{44}$$

We can bound p by observing that $\langle \frac{\nabla S(x_t)}{\|\nabla S(x_t)\|_2}, u \rangle^2$ is a Beta distribution $\mathcal{B}(\frac{1}{2}, \frac{d-1}{2})$:

$$p = \mathbb{P}(|\nabla S(x_t)^T u| < w)$$

$$= \mathbb{P}\left(\langle \frac{\nabla S(x_t)}{\|\nabla S(x_t)\|_2}, u \rangle^2 \leq \frac{w^2}{\|\nabla S(x_t)\|_2^2}\right)$$

$$= \int_0^{\frac{w^2}{\|\nabla S(x_t)\|_2^2}} \frac{x^{-\frac{1}{2}}(1-x)^{\frac{d-3}{2}}}{\mathcal{B}(\frac{1}{2}, \frac{d-1}{2})}dx$$

$$\leq \frac{2w}{\mathcal{B}(\frac{1}{2}, \frac{d-1}{2})\|\nabla S(x_t)\|_2}.$$

Plugging into Equation (44), we get

$$\cos \angle \left(\mathbb{E}[\phi_x(x_t + \delta u)u], \nabla S(x_t) \right)$$

$$\geq 1 - \frac{18w^2}{(\mathbb{E}|\beta_1|)^2 \mathcal{B}(\frac{1}{2}, \frac{d-1}{2})^2 \|\nabla S(x_t)\|_2^2}$$

$$\geq 1 - \frac{9L^2\delta^2}{2(2/(d-1))^2 \|\nabla S(x_t)\|_2^2}$$

$$= 1 - \frac{9L^2\delta^2(d-1)^2}{8\|\nabla S(x_t)\|_2^2}$$

We also observe that

$$\mathbb{E}\widetilde{\nabla S}(x_t, \delta) = \mathbb{E}[\phi_x(x_t + \delta u)u].$$

As a consequence, we have established

$$\cos \angle \left(\mathbb{E}[\widetilde{\nabla S}(x_t, \delta)], \nabla S(x_t) \right) \geq 1 - \frac{9L^2\delta^2(d-1)^2}{8\|\nabla S(x_t)\|_2^2}.$$

Taking $\delta \to 0$, we get

$$\lim_{\delta \to 0} \cos \angle \left(\mathbb{E}[\widetilde{\nabla S}(x_t, \delta)], \nabla S(x_t) \right) = 1.$$

A.3   Proof of Theorem 3

Proof. For notational simplicity, we denote $\xi_b := \phi_x(x_t + \delta u_b)$, and $\bar{\xi} = \frac{1}{B}\sum_{b=1}^{B}\xi_b = \overline{\phi_x}$. We use ξ, u to denote i.i.d. copies of ξ_b and u_b respectively. The variance of the estimate with the baseline is

$$\mathrm{Var}(\widehat{\nabla S}(x_t, \delta)) = \mathbb{E}\left\langle \widehat{\nabla S}(x_t, \delta) - \mathbb{E}\widehat{\nabla S}(x_t, \delta), \widehat{\nabla S}(x_t, \delta) - \mathbb{E}\widehat{\nabla S}(x_t, \delta) \right\rangle$$

$$= \frac{1}{(B-1)^2}\left\langle \sum_{b=1}^{B}\xi_b u_b - \frac{B-1}{B}\mathbb{E}[\xi u] - \bar{\xi}u_b, \sum_{b=1}^{B}\xi_b u_b - \frac{B-1}{B}\mathbb{E}[\xi u] - \bar{\xi}u_b \right\rangle$$

$$= \frac{1}{(B-1)^2}\sum_{a,b=1}^{B}\left\langle \xi_a u_a - \mathbb{E}[\xi u] - (\bar{\xi}u_a - \frac{1}{B}\mathbb{E}[\xi u]), \xi_b u_b - \mathbb{E}[\xi u] - (\bar{\xi}u_b - \frac{1}{B}\mathbb{E}[\xi u]) \right\rangle$$

When $a \neq b$, the summand can be simplified by independence of u_a, u_b and independence of $\xi_a u_a, \xi_b u_b$. In fact,

$$\mathbb{E}\left\langle \xi_a u_a - \mathbb{E}[\xi u] - (\bar{\xi}u_a - \frac{1}{B}\mathbb{E}[\xi u]), \xi_b u_b - \mathbb{E}[\xi u] - (\bar{\xi}u_b - \frac{1}{B}\mathbb{E}[\xi u]) \right\rangle$$

$$= -2\mathbb{E}\left\langle \xi_a u_a - \mathbb{E}[\xi u], \bar{\xi}u_b - \frac{1}{B}\mathbb{E}[\xi u] \right\rangle + \mathbb{E}\left\langle \bar{\xi}u_a - \frac{1}{B}\mathbb{E}[\xi u], \bar{\xi}u_b - \frac{1}{B}\mathbb{E}[\xi u] \right\rangle$$

$$= -2\mathbb{E}\left\langle \xi_a u_a - \mathbb{E}[\xi u], \frac{\xi_a + \xi_b}{B}u_b - \frac{1}{B}\mathbb{E}[\xi u] \right\rangle + \mathbb{E}\left\langle \frac{\xi_a + \xi_b}{B}u_a - \frac{1}{B}\mathbb{E}[\xi u], \frac{\xi_a + \xi_b}{B}u_b - \frac{1}{B}\mathbb{E}[\xi u] \right\rangle$$

$$= -\frac{2}{B}\mathbb{E}\xi_a^2 \left\langle u_a, u_b \right\rangle - 2\mathbb{E}\left\langle \xi_a u_a - \mathbb{E}[\xi u], \frac{\xi_b}{B}u_b - \frac{1}{B}\mathbb{E}[\xi u] \right\rangle + \mathbb{E}[\frac{(\xi_a + \xi_b)^2}{B^2}\langle u_a, u_b \rangle] - \frac{2}{B}\mathbb{E}[\xi u]\mathbb{E}[\frac{\xi_b}{B}u_b] + \frac{1}{B^2}\|\mathbb{E}[\xi u]\|_2^2$$

$$= 0 + 0 + (\frac{2}{B^2} - \frac{2}{B^2} + \frac{1}{B^2})\|\mathbb{E}[\xi u]\|_2^2$$

$$= \frac{1}{B^2}\|\mathbb{E}[\xi u]\|_2^2.$$

When $a = b$, each summand becomes:

$$\mathbb{E}\left\|\xi_a u_a - \mathbb{E}[\xi u] - (\bar{\xi} u_a - \frac{1}{B}\mathbb{E}[\xi u])\right\|_2^2$$

$$= \mathbb{E}\left\|\xi_a u_a - \mathbb{E}[\xi u]\right\|_2^2 - 2\mathbb{E}\left\langle \xi_a u_a - \mathbb{E}[\xi u], \bar{\xi} u_a - \frac{1}{B}\mathbb{E}[\xi u]\right\rangle + \mathbb{E}\|\bar{\xi} u_a - \frac{1}{B}\mathbb{E}[\xi u]\|_2^2$$

$$= \mathbb{E}\left\|\xi_a u_a - \mathbb{E}[\xi u]\right\|_2^2 - 2\mathbb{E}\left\langle \xi_a u_a, \bar{\xi} u_a\right\rangle + \frac{2}{B}\|\mathbb{E}[\xi u]\|_2^2 + \mathbb{E}\|\bar{\xi} u_a\|_2^2 - \frac{2}{B}\left\langle\mathbb{E}[\bar{\xi} u_a], \mathbb{E}[\xi u]\right\rangle + \frac{1}{B^2}\|\mathbb{E}[\xi u]\|_2^2$$

$$= \mathbb{E}\left\|\xi_a u_a - \mathbb{E}[\xi u]\right\|_2^2 - 2\mathbb{E}[\bar{\xi}\xi_a] + \mathbb{E}\bar{\xi}^2 + \frac{2B-1}{B^2}\|\mathbb{E}[\xi u]\|^2.$$

Therefore, the variance can be written as

$$\mathrm{Var}(\widehat{\nabla S}(x_t, \delta)) = \frac{1}{(B-1)^2}\sum_{a=1}^{B}\left(\mathbb{E}\left\|\xi_a u_a - \mathbb{E}[\xi u]\right\|_2^2 - 2\mathbb{E}[\bar{\xi}\xi_a] + \mathbb{E}\bar{\xi}^2 + (\frac{2}{B} - \frac{1}{B^2})\|\mathbb{E}[\xi u]\|^2\right) + \frac{\|\mathbb{E}\xi u\|_2^2}{B(B-1)}$$

$$= \frac{B^2 \mathrm{Var}(\widetilde{\nabla S}(x_t, \delta))}{(B-1)^2} - \frac{B\mathbb{E}[\bar{\xi}^2]}{(B-1)^2} + \frac{(3B-2)\|\mathbb{E}[\xi u]\|_2^2}{B(B-1)^2}$$

$$\leq \frac{B^2 \mathrm{Var}(\widetilde{\nabla S}(x_t, \delta))}{(B-1)^2} - \frac{B\mathbb{E}[\bar{\xi}^2]}{(B-1)^2} + \frac{3B-2}{B(B-1)^2}. \tag{45}$$

The middle term can be expanded as

$$-\frac{B}{(B-1)^2}\mathbb{E}[\bar{\xi}^2]$$

$$= -\frac{B}{(B-1)^2}\sum_{a,b=1}^{B}\mathbb{E}[\xi_a\xi_b]$$

$$= -\frac{1}{(B-1)^2 B}\left(B \cdot 1 + B(B-1) \cdot (2\mathbb{E}\xi - 1)^2\right)$$

$$= -\frac{1}{(B-1)^2} - \frac{4}{B-1}(\mathbb{E}\xi - \frac{1}{2})^2)$$

Plugging into Equation (45), we get

$$\mathrm{Var}(\widehat{\nabla S}(x_t, \delta)) \leq \frac{B^2}{(B-1)^2}\mathrm{Var}(\widetilde{\nabla S}(x_t, \delta)) + \frac{2}{B(B-1)}(1 - 2B(\mathbb{E}[\xi] - \frac{1}{2})^2)$$

$$= \mathrm{Var}(\widetilde{\nabla S}(x_t, \delta))\left\{1 + \frac{2B-1}{(B-1)^2} - \frac{2}{\sigma^2(B-1)}\left(2B(\mathbb{E}[\xi] - \frac{1}{2})^2 - 1\right)\right\}.$$

When $\mathbb{E}[\xi]$ satisfies $(\mathbb{E}[\xi] - \frac{1}{2})^2 > \frac{1}{2B}(1 + \frac{2B-1}{2B-2}\sigma^2)$, we have

$$\frac{2B-1}{(B-1)^2} < \frac{2}{\sigma^2(B-1)}(2B(\mathbb{E}[\xi] - \frac{1}{2})^2 - 1),$$

which implies $\mathrm{Var}(\widehat{\nabla S}(x_t, \delta)) < \mathrm{Var}(\widetilde{\nabla S}(x_t, \delta))$.

$\square$

B Connection to existing white-box attacks

In this subsection, we discuss the connection between our proposed updates (7) and (8), and existing white-box attacks.

Connecting the update (7) **to penalty methods**   A common approach to the constrained problem (2) is to approximate it with a penalty function formulation [43]:

$$\min_x \frac{1}{2}\|x - x^\star\|_2^2 - \rho S_{x^\star}(x), \tag{46}$$

for a carefully chosen penalty parameter ρ. A similar relaxation has been proposed in previous work in adversarial attacks [1, 6].

At the tth step, the update of gradient descent is

$$
\begin{aligned}
x_{t+1} &= x_t - \alpha_t((x_t - x^\star) - \rho_t \nabla S_{x^\star}(x_t)) \\
&= \alpha_t x^\star + (1 - \alpha_t)\Big(x_t + \frac{\rho_t}{1 - \alpha_t}\nabla S_{x^\star}(x_t))\Big) \\
&= \Pi^2_{x^\star, \alpha_t}\Big(x_t + \underbrace{\frac{\rho_t\|\nabla S_{x^\star}(x_t)\|_2}{1 - \alpha_t}}_{\xi_t}\frac{\nabla S_{x^\star}(x_t)}{\|\nabla S_{x^\star}(x_t)\|_2}\Big),
\end{aligned}
$$

where we rewrite the gradient update as a weighted average of the original sample $x^\star$ and the t-th update x_t perturbed along the direction of $\nabla S_{x^\star}(x_t)$ with an appropriately chosen size ξ_t. This has exactly the same form as our proposed update, Equation (6). However, the hyperparameters α_t and ρ_t in previous work [1, 6] are often chosen via hyperparameter tuning or fixed as constant. Here, we choose choose α_t so that x_{t+1} is at the boundary $S(x_{t+1}) = 0$, which is a requirement to use our proposed gradient estimate to be introduced in Section 4.

Connecting the update (8) **to projected gradient descent**   In the untargeted case, each update of Basic Iterative Method proposed by Kurakin et al. [3] is of the form

$$x_{t+1} = \text{Clip}_{x^\star, \alpha_t}\{x_t + \xi_t \text{sign}(\nabla_x J(x_t, c_{\text{true}}))\}, \tag{47}$$

where J is the cross-entropy loss with respect to the true label $c^\star = C(x^\star)$. The operator $\text{Clip}_{x^\star, \alpha}$ performs per-pixel clip within the α-neighborhood of the corresponding pixel of $x^\star$. As pointed out by Madry et al. [7], the Basic Iterative Method can be interpreted as projected gradient descent in the ℓ_∞-norm.

We observe that the clip operator coincides with the ℓ_∞-projection operator $\Pi^\infty_{x^\star, \alpha}$. The cross entropy loss J is a monotonic function of $S_{x^\star}$, and so introduces only a scaling difference between ∇J and $\nabla S_{x^\star}$. As a consequence, apart from the choice of α_t, each update (8) of our algorithm has the same form as the Basic Iterative Method. On the other hand, we need to choose α_t carefully so that x_{t+1} lies at the boundary for gradient-direction estimation.